iScience

CellPress
OPEN ACCESS

Article

Brd2/4 and Myc regulate alternative cell lineage programmes during early osteoclast differentiation in vitro

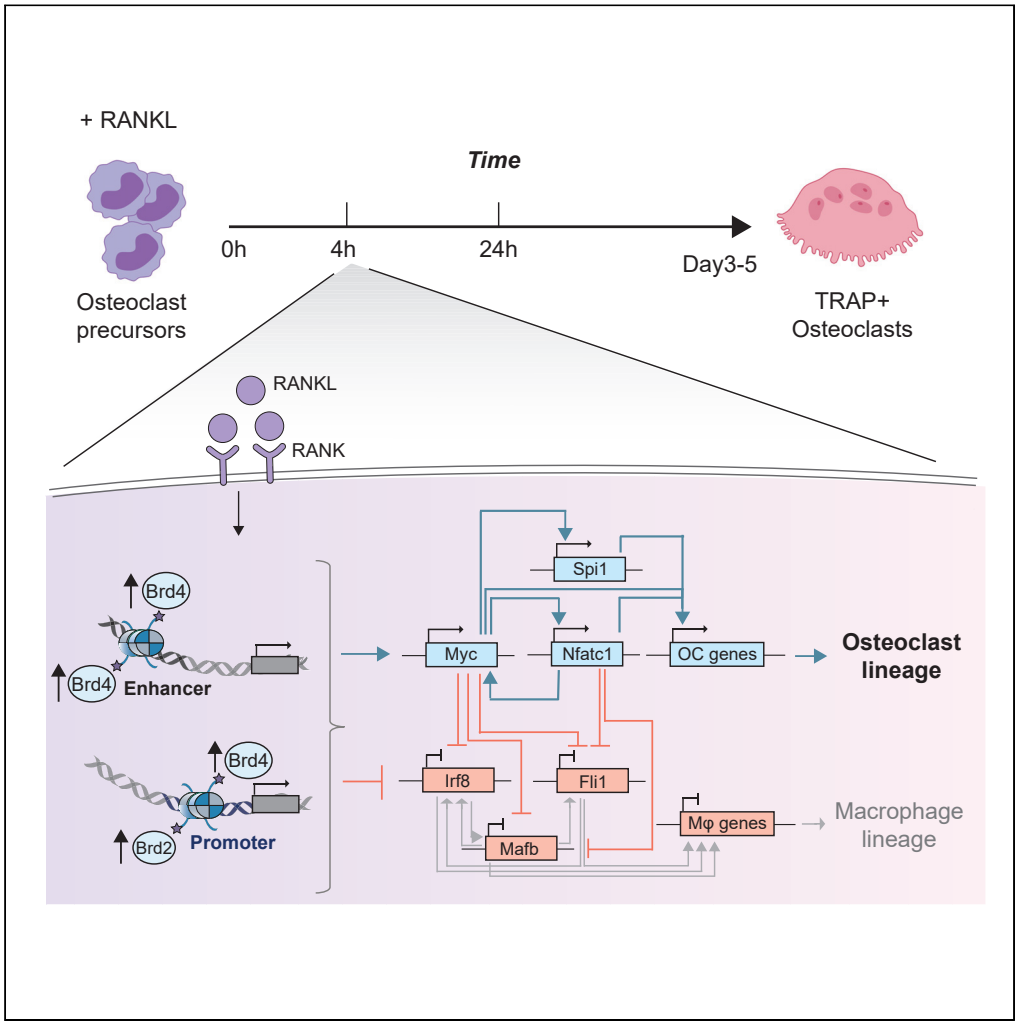

Valentina S. Caputo, Nikolaos Trasanidis, Xiaolin Xiao, ..., Aristeidis Chaidos, Holger W. Auner, Anastasios Karadimitris

a.karadimitris@imperial.ac.uk

HIGHLIGHTS

Upregulation of osteoclast lineage commitment TFs occurs <24hr after RANKL stimulation

Enhanced binding of Brd2&4, but not Brd3, is required for osteoclast fate commitment

Brd2&4 occupancy is associated with super-enhancer reprogramming and TF rewiring

Myc is the epicenter of the TF regulatory network driving osteoclastogenesis

Caputo et al., iScience *24*, 101989
January 22, 2021
https://doi.org/10.1016/j.isci.2020.101989

iScience

CellPress
OPEN ACCESS

Article

Brd2/4 and Myc regulate alternative cell lineage programmes during early osteoclast differentiation in vitro

Valentina S. Caputo,[1,4] Nikolaos Trasanidis,[1,4] Xiaolin Xiao,[1,4] Mark E. Robinson,[1] Alexia Katsarou,[1,2] Kanagaraju Ponnusamy,[1] Rab K. Prinjha,[3] Nicholas Smithers,[3] Aristeidis Chaidos,[1,2] Holger W. Auner,[1,2] and Anastasios Karadimitris[1,2,5,6,*]

SUMMARY

Osteoclast (OC) development in response to nuclear factor kappa-B ligand (RANKL) is critical for bone homeostasis in health and in disease. The early and direct chromatin regulatory changes imparted by the BET chromatin readers Brd2-4 and OC-affiliated transcription factors (TFs) during osteoclastogenesis are not known. Here, we demonstrate that in response to RANKL, early OC development entails regulation of two alternative cell fate transcriptional programmes, OC *vs* macrophage, with repression of the latter following activation of the former. Both programmes are regulated in a non-redundant manner by increased chromatin binding of Brd2 at promoters and of Brd4 at enhancers/super-enhancers. Myc, the top RANKL-induced TF, regulates OC development in co-operation with Brd2/4 and Max and by establishing negative and positive regulatory loops with other lineage-affiliated TFs. These insights into the transcriptional regulation of osteoclastogenesis suggest the clinical potential of selective targeting of Brd2/4 to abrogate pathological OC activation.

INTRODUCTION

Osteoclasts (OCs) are hematopoietic lineage-derived, bone-resorbing cells that in conjunction with bone-forming osteoblasts regulate bone homeostasis in physiology and in disease (Charles and Aliprantis, 2014; Teitelbaum, 2000). Aberrant hyper-activation of OCs underpins common and serious morbidity in osteoporosis and in cancers such as multiple myeloma, metastatic breast, and prostate cancer (Edwards et al., 2008; Le Pape et al., 2016).

OC lineage commitment requires binding of the lineage defining cytokine receptor activator of nuclear factor kappa-B ligand (RANKL) to its receptor RANK expressed in myelomonocytic progenitors in the bone marrow. RANKL-RANK interaction activates a cascade of downstream signal transduction pathways that converge to transcriptional programmes that initiate differentiation and the acquisition of OC-specific processes of cell fusion and polylkaryon generation (Kukita et al., 2004; Yang et al., 2008). This is followed by the maturation events of cytoskeleton re-organization and secretion of collagen-degrading enzymes and hydroxyapatite-dissolving proton ions that enable OCs to resorb organic and inorganic bone (Azuma et al., 2000; Soysa et al., 2012; Teitelbaum, 2000).

OC-specific lineage commitment and differentiation requires a compendium of transcription factors (TFs) that are upregulated in response to RANKL, such as the Fos family, Nfkb, NFATc1, Spi1/Pu.1 (Franzoso et al., 1997; Takayanagi et al., 2002; Wagner, 2002). OC commitment also requires a simultaneous repression of existing macrophage/monocytic, inflammatory transcriptional programmes that involve downregulation of TFs such as Irf8, Mafb, and Bcl6 (Kim et al., 2007; Zhao et al., 2009). These TFs in turn are under the repressive regulation of Blimp1 (*Prdm1*) which is upregulated in response to RANKL (Kurotaki et al., 2020; Miyauchi et al., 2010; Nishikawa et al., 2010).

Similar to other transcriptional processes that define cell lineage commitment, the OC-affiliated TF would be expected to alter gene transcription through changes in the activity of proximal and distal regulatory

[1]Hugh & Josseline Langmuir Centre for Myeloma Research, Centre for Haematology, Department of Immunology and Inflammation, Imperial College London, London, UK

[2]Department of Haematology, Hammersmith Hospital, Imperial College Healthcare NHS Foundation Trust, London, UK

[3]Medicines Research Centre, GlaxoSmithKline, Stevenage, UK

[4]These authors contributed equally

[5]Senior author

[6]Lead contact

*Correspondence: a.karadimitris@imperial.ac.uk

https://doi.org/10.1016/j.isci.2020.101989

DNA elements namely enhancers. The latter are often cell type specific, and their activity is regulated by Brd2-4, the bromodomain and extraterminal domain (BET) proteins which act as chromatin readers and transcriptional activators by binding to acetylated histones (Hnisz et al., 2013) (Chiang, 2009; LeRoy et al., 2008; Rahman et al., 2011).

Previous work demonstrated the requirement for Brd4 for OC activation in response to RANKL while BET protein inhibitors inhibit OCs *in vivo* as well as *in vitro* and protect from malignancy- or ovariectomy-induced bone disease (Lamoureux et al., 2014; Park-Min et al., 2014). Further, Brd4 binds to the promoters of lineage-defining TFs, such as *Nfatc1*, *cFos*, and *NF-κB*, while pharmacological inhibition by BET inhibitors represses transcription of these TFs (Lamoureux et al., 2014). More recently, the role of Myc in OC differentiation was highlighted and was shown to be required for OC development by regulating transcription of *Nfatc1* and *Errα* (Bae et al., 2017; Lamoureux et al., 2014) (Park-Min et al., 2014).

Despite this progress, how individual BET proteins, singly or in combination, regulate commitment to OC lineage genome-wide at the chromatin level and their interplay with Myc have not been addressed (Baud'huin et al., 2017; Lamoureux et al., 2014; Park-Min et al., 2014). Here, we first identify the initiating regulatory events leading to OC lineage commitment and demonstrate a prominent and non-redundant role of Brd2 and 4 in the chromatin changes underlying these processes. We provide high resolution analysis and integration of the genome-wide binding profile of BET proteins in conjunction with chromatin accessibility maps and early dynamic transcriptome changes in response to RANKL and to BET protein inhibitors. We thus define the combinatorial cross-talk between BET proteins and their interaction with proximal and distant chromatin regulatory areas to define the early stages of OC lineage commitment. Further, we generate the gene regulatory networks (GRNs) driving OC lineage commitment and identify critical TF components defining OC fate determination. We validate the role of Myc as a major hub in these OC-specific GRNs and discover the range of its transcriptional targets and their predicted functions.

RESULTS

A dynamic map of early transcriptome changes in response to RANKL

To model OC lineage commitment in response to RANKL, we used the mouse macrophage cell line RAW264.7 which upon RANKL exposure differentiates to fully bone-resorbing OCs (Collin-Osdoby and Osdoby, 2012; Collin-Osdoby et al., 2003; Raschke et al., 1978). We confirmed that differentiation of RAW264.7 cells, as well as of murine primary bone marrow and purified bone marrow (Lineage^{-}CD115^{+}cKit^{+}) progenitor cells (Hu et al., 2011) toward OCs, was inhibited by the pan-BET protein inhibitor I-BET151 (Figures S1A and S1B) (Baud'huin et al., 2017; Park-Min et al., 2014).

Transcriptome changes brought about 24h after RANKL treatment of RAW264.7 cells correlated highly with those induced by RANKL on OC developing from primary bone marrow (BM) progenitors/precursors (Bae et al., 2017) (Figure S1C), thus attesting further to the suitability of RAW264.7 cells as a model of OC development.

While transcriptome analysis of developing OC has been previously reported at >24h post-RANKL exposure (An et al., 2014; Bae et al., 2017; Davidson et al., 2020; Park-Min et al., 2014), the immediate transcriptional responses triggered by RANKL have not been explored yet. Therefore, to capture the first transcriptional waves during RANKL-driven OC lineage commitment, we performed RNA-seq of RAW264.7 cells at 0, 4, 14, and 24h upon RANKL, I-BET151, and RANKL + I-BET151 treatment (Figure 1A). In addition, we investigated the genome-wide recruitment dynamics of the Brd2-4 proteins that are associated with early transcriptional changes at 4h after treatment (Figure 1A).

Upon RANKL treatment, we identified 12 clusters (C1-C12) of differentially expressed genes (DEGs; Figures 1B and 1C) temporally categorized as early (4hr) and late (14 and 24hr). The largest, C6 (late repressed), comprises 780 genes and includes TFs (e.g. *Irf8*, *Mafb*, and *Bcl6*) whose repression is required for extinguishment of the non-permissive macrophage/monocytic transcriptional programmes, thus allowing OC lineage commitment (Figure 1C and Table S1). The early activated C10 contains the OC differentiation master regulators *Nfatc1*, *Fos*, and *Myc*, followed by the upstream repressor of macrophage lineage *Blimp1/Prdm1*. Using quantitative PCR (qPCR), we confirmed this dynamic, contrasting *Myc* and *Irf8* mRNA expression pattern in murine primary bone-marrow-derived pre-OCs (Figure S1D).

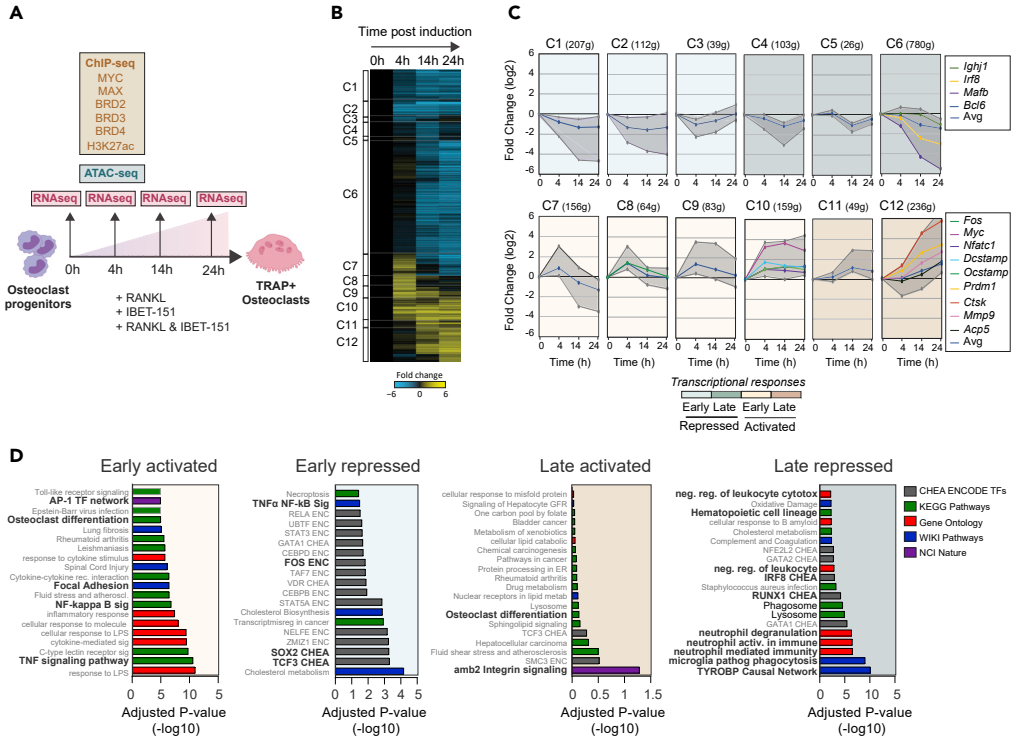

Figure 1. Profiling the dynamics of transcriptional responses underlying early osteoclast development in response to RANKL

(A) Schematic representation of the study outline. RNA-seq analysis performed at 0, 4, 14, and 24 hr after RANKL induction in RAW 264.7 cells. Gene clusters (C1-C12), comprising four main modes of transcriptional response: early repressed; late repressed; early activated; late activated.

(B–D) Heatmap (B) and line graphs (C) illustrate for the transcriptional patterns observed in the 12 clusters; the expression patterns of genes with prominent role in osteoclastogenesis are also highlighted here. Overrepresentation analysis (D) using EnrichR online tool depicts the involvement of key pathways in the four modes of responses.

Principal component (PCA) and intesity-ratio (MA) analysis showed a profound impact of I-BET151 in abrogating RANKL-dependent transcriptome changes as early as 4hr after treatment (Figure S1E). These findings confirm the exquisite sensitivity of the RANKL-dependent OC-defining transcriptional programme to BET inhibitors and its dependency on BET proteins. A high-resolution dynamic analysis of *Nfatc1* expression further exemplified the dramatic impact of BET inhibitors in the transcriptional regulation of OC lineage commitment (Figure S2A).

Pathway enrichment analysis of early activated clusters C7-C10 was consistent with effects of RANKL-mediated osteoclastogenesis and activation of downstream pathways such as NF-κB, TNFα, and AP-1 (i.e., c-Jun/c-Fos). Of note, among the early activated clusters, and in particular in C7, gene repression at 14 and 24 hr is preceded by increased expression at 4 hr. Pathway enrichment analysis of the 156 C7 genes showed enrichment for putative gene targets of Irf8 in bone marrow macrophages and for genes that define macrophage identity (Figure S2B). This suggests that before definitive repression of the macrophage transcriptional programme occurs, RAW264.7 cells assume a state of transient transcriptional transition to an immature macrophage identity.

Late repressed genes reflected loss of phagocytic capacity and notably decreased expression of genes predicted to be regulated by Irf8 in mouse macrophage cells (Figure 1D).

Notably, genes such as *Dcstamp*, *Ocstamp*, and *Atp6v0d2* that are required for polykaryon formation, a cellular process that starts at least 48 h after RANKL exposure (Kukita et al., 2004; Wu et al., 2009; Yang et al., 2008), also map to the same early cluster as the master TF (Figure 1B and 1C). In addition, genes such as *Ctsk* and *Mmp9*, which are associated with acquisition of OC bone resorptive capacity, a cellular

feature present in developing OC after 3 days (Boyce, 2013; Hsu et al., 1999; Sundaram et al., 2007; Troen, 2006), are upregulated at 4–14 hr (Figures 1B and 1C). Therefore, our early post-RANKL transcriptome analysis reveals that transcription of genes required for functions of maturing or mature OC is already active within a few hours following RANKL exposure, a finding that we validated by qPCR Sin primary pre-OCs for *Dcstamp* and *Ocstamp* (Figure S1D).

Overall, inspection of all 12 clusters reveals that transcriptome analysis at 14 h after RANKL treatment captures both the early and late transcriptional events that define RANKL-induced OC lineage commitment and differentiation that entails activation of the osteoclastogenic program followed by repression of the macrophage program.

Of note, while double RANKL/I-BET151 treatment reverses the RANKL-induced transcriptional changes, I-BET151 alone represses both alternative cell fate programmes (Figure S2C; OC C10, C12 gene clusters and macrophage C6 cluster) consistent with the role of BET proteins in determining cell fate decisions in development (Huijbregts et al., 2019) (Fernandez-Alonso et al., 2017; Hnisz et al., 2013; Lee et al., 2017). We validated this effect of RANKL/I-BET151 and I-BET151 treatment in primary pre-OCs by measuring expression of genes of interest (Figure S2D). Indeed, while expression of *Irf8* increased significantly after 4 hr of treatment with RANKL/I-BET151 and I-BET151, that of *Myc*, *Dcstamp*, and *Ocstamp* was significantly decreased, consistent with the repressive role of BET proteins in the regulation of *Irf8* and activating role in the regulation of the other three genes.

Impact of RANKL and I-BET151 on early chromatin recruitment of Brd2-4

To map RANKL- and I-BET151-induced changes in Brd2-4 chromatin binding, we obtained the genome-wide binding profile of the three BET proteins at steady state (S) and at 4h after RANKL (R), RANKL plus I-BET151 (RI), or I-BET151(I) treatment using Chromatin Immunoprecipitation followed by sequencing (ChIP-seq).

By first plotting the average ChIP signal against fold change between R and S conditions (R/S), we identified the differentially enhanced or decreased peaks in R condition for each of the BET proteins. This analysis (Figure 2A and Table S2) demonstrated that RANKL induces mostly increased binding of Brd2 and 4 with minor and nearly equal increase and reduction in binding of Brd3. Overall, 45% of Brd2 and 52% of Brd4 peaks in RANKL-treated cells represented enhanced differentially binding sites (DBSs), while the corresponding fraction for Brd3 was <21% (Figure 2B). However, I-BET151 induced a profound reduction in the binding of all three BET proteins, more pronounced for Brd4 (99%) and less so for Brd2 (75%) and Brd3 (71%) (Figure 2B). Of note, in contrast to Brd3 and 4, a preferential increase in biding of Brd2 was observed in I-BET-only treated cells but not in RANKL+I-BET cells (Figures 2A and 2B). Interestingly, among BET protein genes, expression of *Brd2* is the only one that increases in response to I-BET151 treatment (Figures S3A and S3B).

Genomic feature annotation of the DBS revealed that dynamic changes of Brd4 mostly take place in intronic and intergenic areas, while Brd2 and 3 binding changes are mainly enriched in promoter-overlapping areas (Figure 2C). This distribution chimes with the previously described role of Brd4 as a marker of intergenic and intronic enhancers (Loven et al., 2013; Roe et al., 2015). Gain of Brd2 or Brd4 binding occurs with, but mostly without, concurrent Brd4 and Brd2 increased binding, respectively, and in either case, it does not involve changes in Brd3 binding (Figures 2D–2F). We therefore obtained the union of these Brd2 & 4 peak sets to form four DBS categories for further analysis (i.e., unaltered, Brd2&4 common, Brd2 specific, Brd4 specific; Figure 2F).

Feature annotation demonstrated preferential differential binding of sole Brd4 in intergenic and intronic areas, likely enriched in putative enhancers, while Brd2 DBSs alone and in combination with Brd4 DBSs were enriched preferentially in promoter-overlapping areas (Figure 2G).

Overall, these findings show that RANKL brings about changes in the BET protein chromatin-binding landscape at the very first stages of OC commitment (4h), chiefly detected as enhanced binding of Brd2 and Brd4, and such changes are exquisitely sensitive to pharmacological inhibition.

Enhanced Brd2&4 chromatin occupancy and super-enhancer reprogramming in early osteoclastogenesis

To gain further insights into how dynamic changes in Brd2&4 chromatin binding affect the RANKL-induced transcriptome changes, by annotating DBSs to the nearest DEG, we plotted dynamic transcriptional

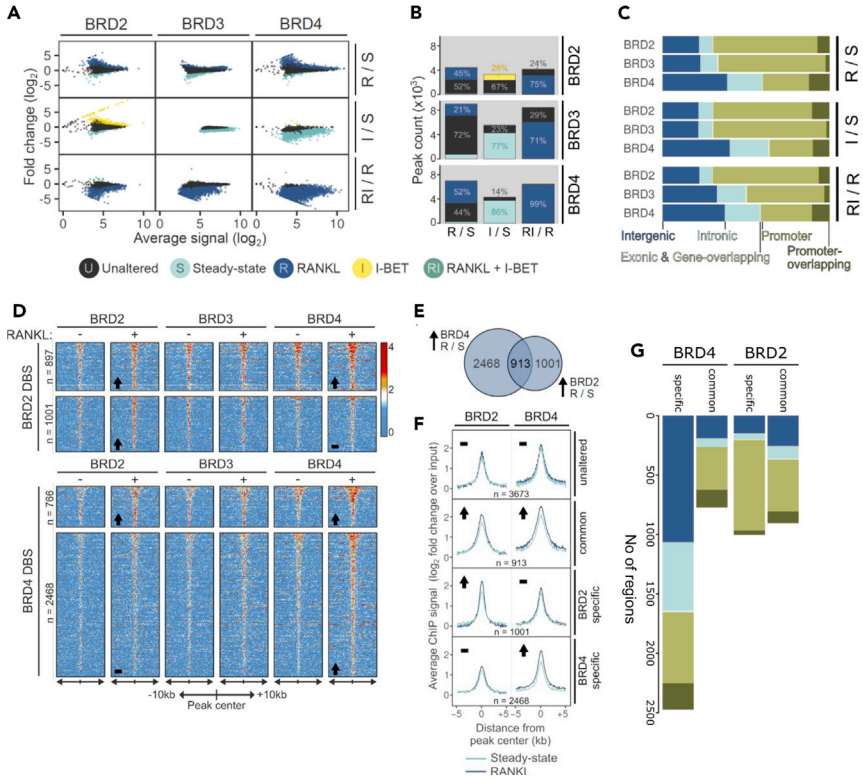

Figure 2. Early epigenomic alterations in chromatin binding of Brd2,3, and 4 in response to RANKL & I-BET

Differential binding of Brd2, Brd3, and Brd4 in response to RANKL (R), I-BET (I), or a combination of the two (RI) was analyzed 4 h after treatment. S: steady state

(A) Ratio-intensity plots of average ChIP signal and differential binding between conditions (log_2 scale) are displayed for each BRD (columns) across treatment contrasts (rows).

(B) Number of differentially bound sites (DBSs) for BET proteins across pairwise treatment comparisons (from A). All DBS are colored by associated condition; non-significantly altered regions are colored gray.

(C) Genomic annotation for all DBS per condition.

(D) Relative enrichment of Brd2,3,4 on Brd2 (top) and Brd4 (bottom) DBSs. Fold change over input in a 20kb window around peak center was plotted for each BRD in S and R conditions, direction of change in Brd2/4 is indicated in lower left corner.

(E) Distribution of DBSs with increased Brd2, Brd4, or dual Brd2,4 enrichment upon RANKL induction.

(F) Average signal profiles for Brd2 and Brd4 across combined differential binding categories, direction of change in Brd2/4 is indicated in top left corner of each group.

(G) Genomic annotation of Brd2/4 binding locations relative to gene features in Brd2/Brd4 common or specific binding.

changes associated with each BET protein DBS categories, i.e., common, Brd2 specific, or Brd4 specific. This analysis revealed that for each group, enhanced binding was associated with the same pattern of transcriptional changes that included up- as well as down-regulated genes (Figure S4A).

Functional annotation of DEGs upon RANKL treatment shows that each of the three DBS categories contributes to the same or unique pathways and TF networks that define OC development (Figure 3A). These included up-regulation of genes involved in Myc, TNF, Nfkb, MAPK, and other OC differentiation pathways, as well as repression of genes involved in commitment to the alternative monocyte-macrophage lineage, e.g. *Runx1*, *Spi1*, and *Irf8* pathways.

To explore how the dynamic changes in Brd2 and 4 binding might interact with the TF in mediating RANKL-induced transcriptome changes for each of the three DBS categories, we correlated changes in TF expression with proportion of DBS enriched in TF motifs (Figure 3B and 3C). This analysis predicted that at 4 hr, sole Brd2 and Brd4 rather than their combined enhanced binding was associated with motif enrichment of TFs that determine alternative cell fates, i.e., Irf8, Fli1, and Mafb, which are downregulated in response to RANKL versus the RANKL-activated, OC-activating TF Fosl1/2, Junb, Myc, Nfkb2, Spi1, and Relb.

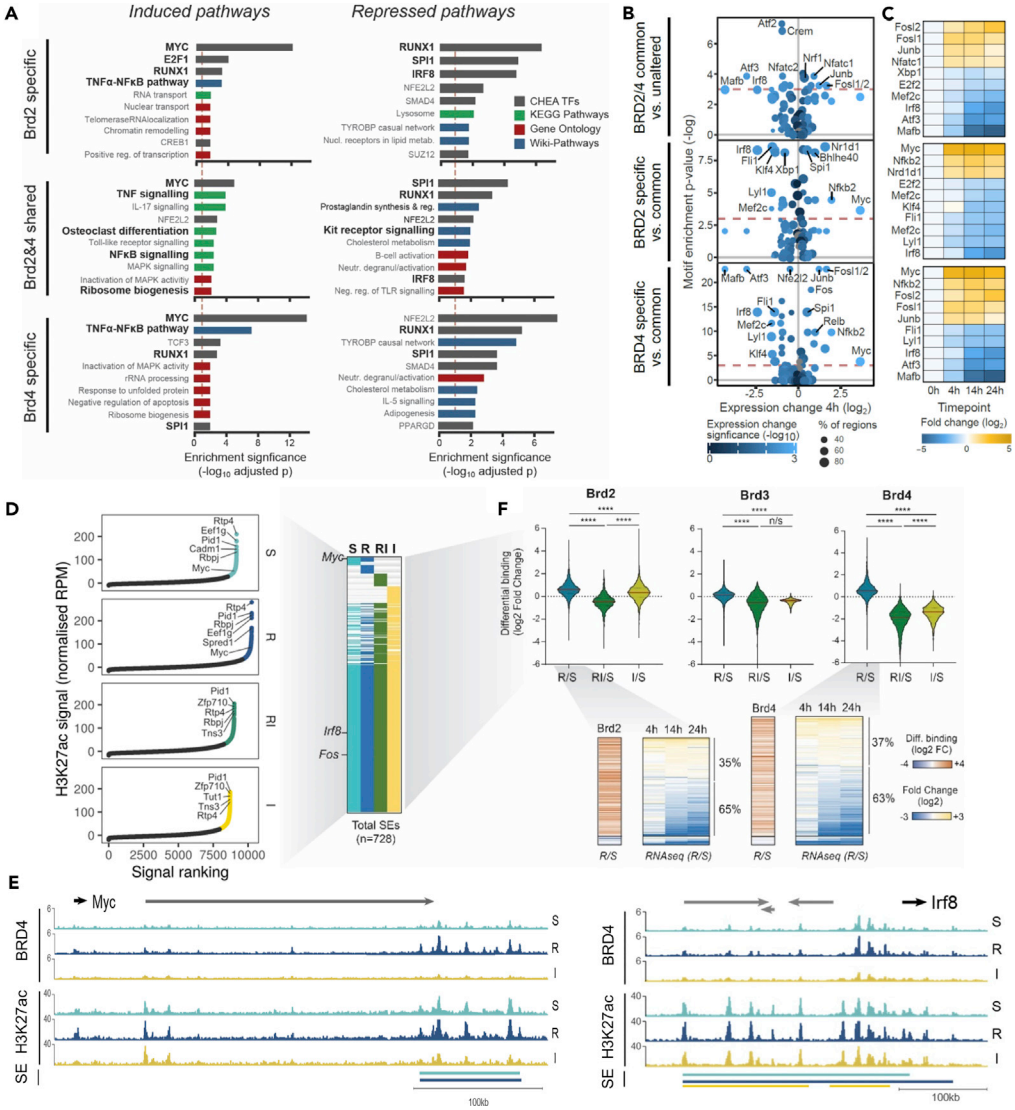

Figure 3. Differential Brd2 and Brd4 chromatin occupancy is linked to early transcriptional responses and super-enhancer reprogramming in osteoclast differentiation

(A) Top 10 enriched pathways for up- and down-regulated genes (4, 14, and 24hr after RANKL induction) associated with each Brd2/4 binding category (Brd2 specific, Brd4 specific, or shared); color indicates database source for gene set.

(B) Relative motif enrichment per Brd2/4 binding category against either unaltered regions to identify commonly enriched factors (top) or against common regions (middle, bottom) to identify Brd2/4-specific factors. Enriched motifs were grouped by similarity and assigned to putative TFs based on the expression level and differential expression at 4h. Size indicates proportion of regions containing the motif, and color indicates significance of expression change.

(C) Differential expression patterns (RANKL-treated vs untreated) for top 10 TFs predicted to be involved in Brd2/4 regulation of osteoclastogenesis.

(D) Super-enhancer (SE) calling in S, R, RI, and I conditions using H3K27ac ChIPseq.

(E) Epigenomic alterations in genetic loci of the hallmark osteoclastogenesis genes *Irf8* and *Myc*, across treatments.

(F) Relative occupancy (R vs S, RI vs S, and I vs S) of Brd2,3,4 on SE sites (top); time course transcriptional changes associated with differential Brd2,4 binding after RANKL induction (bottom). One-way ANOVA test: ****,$p < 0.0001$; n/s, not significant.

Together, these data suggest a non-redundant epigenetic role of Brd2 and Brd4 in OC lineage commitment and differentiation in co-operation with lineage-defining TFs.

Next, by charting the chromatin H3K27ac enrichment load, we sought to identify super-enhancers (SEs), i.e., the regulatory elements that determine cell fate decisions by regulating and being regulated by

lineage-affiliated TFs (Figure 3D) often in co-operation with Brd4 (Bae et al., 2017; Loven et al., 2013; Whyte et al., 2013). In total, we identified 728 SEs across different treatments, more than half of which were shared in all four conditions (Figures 3D and Table S3). The majority of SEs which regulate critical TFs (e.g. *Irf8*, *Fos*; Figures 3E and S4B) remained unaltered in terms of H3K27ac load across treatments; however, in a few SEs (including the one of *Myc*), H3K27ac load was reduced upon I-BET151 treatment (Figures 3D and 3E). By contrast, analysis of the BET protein binding load at these SEs confirmed significantly increased binding of both Brd2 and 4 (but not of Brd3) upon RANKL treatment, while I-BET151 treatment resulted in significantly reduced binding of Brd2-4 proteins at SEs (Figures 3E, 3F, and S4B). This effect of I-BET151 was more pronounced for Brd4 and is consistent with its previously described role in SEs (Loven et al., 2013).

Notably, increased binding of Brd2/4 at SEs was associated mostly with transcriptional repression (65% of DEGs) rather than activation (35% of DEGs) of the predicted target genes at 14 and 24 hr (Figure 3F).

Pathway enrichment of DEGs predicted to be upregulated upon differential binding of Brd2&4 to enhancers and SEs confirmed activation of OC differentiation and TNF-α/Nfkb pathways, respectively, while repression of Irf8 targets genes was predicted among down-regulated genes (Figures S4C and S4D)

Thus, in a non-redundant manner, Brd2 and Brd4 via their enhanced binding in response to RANKL and in co-operation of lineage-affiliated TFs determine cell OC lineage commitment and fate by exerting dual, repressive as well activatory transcriptional roles.

Myc is the epicenter of the OC lineage commitment gene regulatory network

By taking advantage of the ability afforded by ATAC-seq (Assay for Transposase-Accessible Chromatin using sequencing) to identify footprints of DNA binding factors, we obtained and annotated genome-wide footprints of expressed TFs at promoters and enhancers in RANKL-treated RAW264.7 cells. This identified high confidence footprints of several OC-associated TFs (Figure S5A) and allowed construction of a TF-focused GRN.

By displaying the highest expression change than any other TF in response to RANKL (Figure S5B), Myc appears central in the TF-driven GRN of OC lineage commitment (Figure 4A). We confirmed by qPCR that overexpression of *Myc* in response to RANKL is (a) higher than that of *Nfatc1* and (b) it is BET protein dependent, as shown by abrogation of *Myc* overexpression (Figure S5B) and reduction in Brd2/4 binding at the predicted *Myc* SE upon I-BET151 treatment (Figure 3E).

A closer inspection of the GRN reveals that Myc is regulated by Nfatc1, Fosl2, and Nfkb2 while it is predicted to repress *Irf8* and *Mafb* (Figures 4A, 4B, and S5C). Notably, Myc is predicted to establish positive feedback loops with TFs that promote OC differentiation (e.g., Nfatc1, Figure 4B) and a negative feedback loops with TFs that activate the macrophage program (e.g., Irf8 and Mafb, Figure 4B). These findings are consistent with previous low throughput analyses of the role of Brd2/4 proteins in regulating expression of both *Myc* and *Nfatc1* in OC and the Myc requirement for *Nfatc1* upregulation in response to RANKL (Lamoureux et al., 2014; Park-Min et al., 2014).

Despite the critical role of Myc in OC development, its genome-wide regulatory landscape in response to RANKL is not known. Herein, we first confirmed that Myc depletion by shRNA or by the Myc/Max dimerization inhibitor 10,058–F4 (Yu et al., 2016) inhibited osteoclastogenesis (Figures S6A and S6B).

Next, we performed ChIP-seq against Myc and its partner Max 4h after RANKL treatment in RAW264.7 cells. Myc binding was equally enriched between putative intergenic and intronic enhancers and proximal regulatory areas. We identified 560 Myc areas also co-bound by Max (Figures 4C and 4D and Table S4); these areas were highly enriched in Fli1, Fosl2, Pu.1/Spi1, Irf8, as well as Myc and Max motifs, supporting a co-operative function of these TFs with Myc in OC development at the genome-wide level (Figure 4E). Over-representation analysis of DEGs predicted to be regulated by Myc/Max binding showed activation of genes involved in ribosome-related pathways, as well as of previously known Myc/Max targets, and repression of Irf8, Runx1, and Spi1/Pu.1 targets (Figure 4F). Moreover, we identified the OC pioneer factor *Spi1* and *Fli1* as direct targets of Myc, as predicted by the presence of Myc footprints and ChIP-seq peaks at their corresponding SE (Figures 4A and 4G); interestingly, binding of Irf8 and Spi1 on the same SE was previously described to promote macrophage-lineage commitment (Langlais et al., 2016), while the alternative Spi1/Nfact1 partnership favors OC lineage commitment (Carey et al., 2018; Izawa et al., 2019) (Kurotaki et al., 2020).

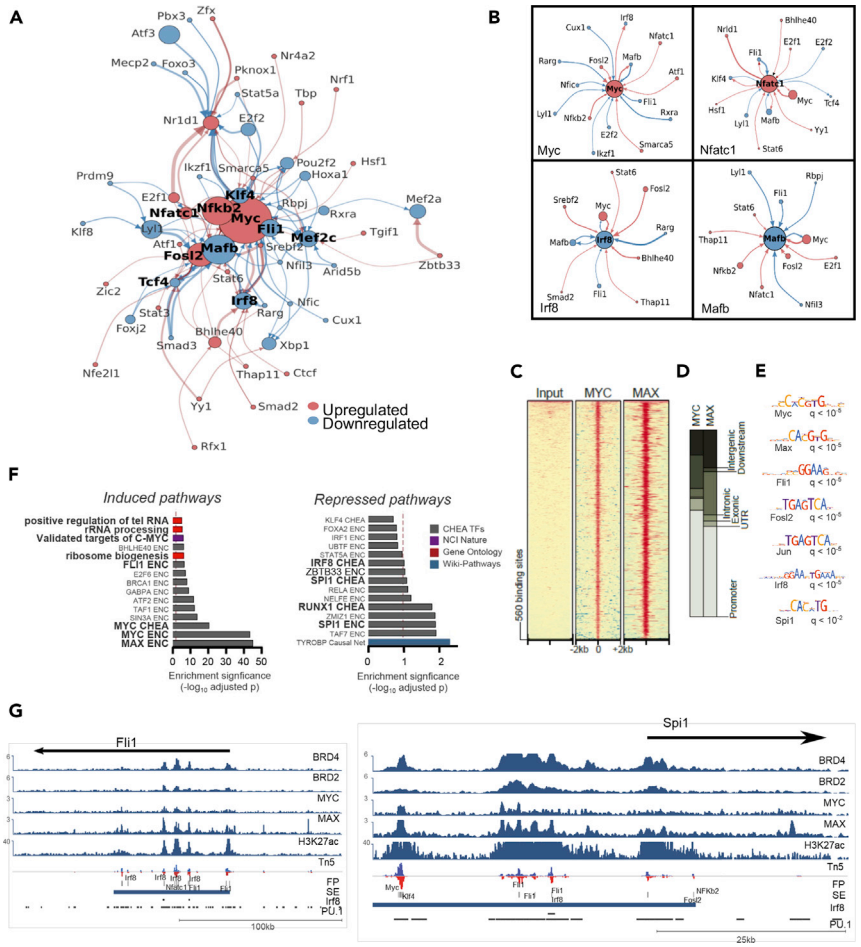

Figure 4. Myc is a central component of the regulatory networks driving osteoclast-lineage commitment

(A) Chromatin accessibility-based construction of gene regulatory network that drives transcriptional changes during OC lineage commitment. Directed TF network diagram: arrow width indicates footprint score for originating TFs at target gene promoter/enhancer, and color indicates direction of expression change for originating TFs (red: upregulated and blue: downregulated). Node size indicates strength of expression change ($-\log_{10}(padj)*|\log_2 FC|$) and color indicates direction of change at 14 hr after RANKL treatment.

(B) Individual TF modules comprising core components of the overall network.

(C–E) (C) Heatmap representation of ChIP-seq against Myc and Max, along with (D) genomic annotation of significantly enriched areas and (E) thier motif analysis.

(F) Overrepresentation analysis of direct Myc gene targets (as predicted upon integrated cistrome-transcriptome analysis) using EnrichR.

(G) IGV snapshots of *Fli1 and Spi1* genetic loci. From top to bottom: showing Brd2/4, Myc, Max and H3K27Ac ChIP-seq, ATAC-seq and Pu.1. and Irf8 ChiP-seq are from (Langlais et al., 2016).

Integrative epigenomic analysis of the Myc chromatin binding sites revealed significant increase of H3K27ac, Brd2, and Brd4 (but not Brd3) occupancy upon RANKL treatment (Figure S6C). Although no significant change in H3K27ac signal was detected upon RANKL + I-BET151 treatment, Brd2-4 binding signal significantly decreased on the same regions, more prominently for Brd4.

Finally, over-representation analysis of the post-RANKL variable genes predicted to be co-regulated by Myc/Max binding and enhanced binding of BET proteins showed again among upregulated genes the role of Myc in regulating previously identified Myc/Max target genes and in promoting ribosome biology (Figure S6D). Genes predicted to be down-regulated by Myc/Brd2,4 are enriched for Spi1/Pu.1 targets in macrophage cells (Langlais et al., 2016), further supporting a co-operative role of Spi1/Pu.1 with Myc in OC lineage commitment.

Together, these findings show a central role of Myc in OC lineage commitment in co-operation with Brd2/4 and lineage-defining TFs.

DISCUSSION

Here, we dissected the immediate early epigenetic and transcriptional events that are regulated by BET proteins in response to RANKL during OC lineage commitment. Two main insights emerged from the dynamic analysis of the OC transcriptome. First, regulation of the two competing lineage programmes, i.e., repression of macrophage vs activation of the OC program is temporally dissociated, with the former following the latter. This is consistent with the previously described role of Blimp1, a RANKL-activated TF, in repressing Irf8- and Irf8-dependent macrophage-affiliated transcriptional programmes (Miyauchi et al., 2010; Nishikawa et al., 2010). Second, transcriptional activation of genes regulating late functions of OCs, i.e., cell-to-cell fusion and bone resorption, already takes place in the first 24 hr after RANKL exposure, thus providing a paradigm of a cellular differentiation trajectory imprinted in the beginning of the process. Future single-cell-based analyses of developing OCs would provide additional, high-resolution insights into these transcriptional processes.

The non-redundant genetic roles of Brd2 and Brd4 in osteoclastogenesis have been previously shown as has the ability of BET protein inhibitors to abrogate OC development by interfering with transcription of individual critical TF (Baud'huin et al., 2017; Lamoureux et al., 2014; Park-Min et al., 2014). Here, we establish that RANKL induces changes primarily in the binding patterns of Brd2 and Brd4, with the latter mainly focused on enhancers and SEs. While BET protein function has been primarily linked with gene activation (Chiang 2009), our findings clearly show that enhanced Brd2/4 binding in response to RANKL is predicted to mostly regulate repression of the existing macrophage program, highlighting the dual function of Brd2/4 in gene regulation.

Brd2 and Brd4 are predicted to regulate critical pathways for OC development on individual or shared basis, alluding, in line with previous genetic studies (Baud'huin et al., 2017), to a non-redundant functional role in osteoclastogenesis. Therefore, use of selective Brd2 or Brd4 inhibitors would be expected to abrogate pathological, RANKL-dependent OC activation with a more favorable toxicity profile than pan-BET inhibitors such as I-BET151.

Construction of TF-focused GRNs highlighted the role of positive and negative feedback loops of TF cross-regulation with Myc emerging as the most central TF in this process. Indeed, the BET protein-dependent increase in Myc expression is the highest among TFs responding to RANKL. While transcriptome analysis of Myc-deficient OC precursors suggested that Myc regulates metabolic processes such as oxidative phosphorylation in developing OC (Bae et al., 2017) whether relevant genes are directly regulated by Myc binding is not known. Here, we find that Myc is predicted to regulate pro-osteoclastogenic TF such as Nfatc1, Fosl2, and Nfkb2 by establishing positive regulatory loops. In addition, through repression of Irf8 and Mafb and in co-operation with Spi1/Pu.1, Myc participates in the repression of the macrophage transcriptional program required for OC development.

In summary, here we propose a non-redundant role of both Brd2 and 4 which cooperate with Myc to orchestrate early chromatin events and TF regulatory networks that determine OC lineage commitment.

Limitations of the study

Although our study maps the dynamic changes in transcriptional regulation during early osteoclastogenesis in both cell line and primary OC precursor cells, these changes represent average regulatory events at the cell population level and assume synchronous cellular responses upon cytokine stimulation and BET-protein inhibition. Additionally, single-cell epigenomic and transcriptomic analyses could provide further insights into understanding the dynamics of gene expression regulation during OC lineage commitment.

Resource availability

Lead contact

Further requests for resources and materials should be directed to and will be fulfilled by the Lead Contact, Anastasios Karadimitris (a.karadimitris@imperial.ac.uk).

Material availability

This study did not yield new unique reagents.

Data and code availability

Data are available from Gene Expression Omnibus database (Acc. Number: GSE160840).

METHODS

All methods can be found in the accompanying Transparent Methods supplemental file.

SUPPLEMENTAL INFORMATION

Supplemental Information can be found online at https://doi.org/10.1016/j.isci.2020.101989.

ACKNOWLEDGMENTS

V.C., N.T., X.X. and K.P. were supported by the Blood Cancer UK and A.K. was supported by Kay Kendall Leukaemia Fund. We also acknowledge support from Imperial NIHR Biomedical Research Center Genomics Facility, and research funding from GlaxoSmithKline.

AUTHOR CONTRIBUTIONS

V.S.C. and N.T. designed study, performed experiments, and analyzed data. X.X., N.T., and M.R. analyzed data. A.C., K.P., A.K., and H.W.A. provided advice and ideas. A.K. designed study and supervised experiments. V.S.C., N.T., X.X., and A.K. wrote manuscript. All authors contributed to the final draft of the manuscript. N.S. and R.K.P. contributed in provision of compound and related information and reviewed data and the manuscript.

DECLARATION OF INTERESTS

The work was in part supported by received research funding from GlaxoSmithKline to A.K. All the other authors declare no conflict of interest.R.K.P. and N.S. are employees and shareholders of GlaxoSmithKline, which is carrying out clinical development of epigenetic inhibitors.

Received: October 2, 2020
Revised: November 7, 2020
Accepted: December 21, 2020
Published: January 22, 2021

REFERENCES

An, E., Narayanan, M., Manes, N.P., and Nita-Lazar, A. (2014). Characterization of functional reprogramming during osteoclast development using quantitative proteomics and mRNA profiling. Mol. Cell Proteomics *13*, 2687–2704.

Azuma, Y., Kaji, K., Katogi, R., Takeshita, S., and Kudo, A. (2000). Tumor necrosis factor-alpha induces differentiation of and bone resorption by osteoclasts. J. Biol. Chem. *275*, 4858–4864.

Bae, S., Lee, M.J., Mun, S.H., Giannopoulou, E.G., Yong-Gonzalez, V., Cross, J.R., Murata, K., Giguere, V., van der Meulen, M., and Park-Min, K.H. (2017). MYC-dependent oxidative metabolism regulates osteoclastogenesis via nuclear receptor ERRalpha. J. Clin. Invest. *127*, 2555–2568.

Baud'huin, M., Lamoureux, F., Jacques, C., Rodriguez Calleja, L., Quillard, T., Charrier, C., Amiaud, J., Berreur, M., Brounais-LeRoyer, B., Owen, R., et al. (2017). Inhibition of BET proteins and epigenetic signaling as a potential treatment for osteoporosis. Bone *94*, 10–21.

Boyce, B.F. (2013). Advances in the regulation of osteoclasts and osteoclast functions. J. Dent. Res. *92*, 860–867.

Carey, H.A., Hildreth, B.E., 3rd, Geisler, J.A., Nickel, M.C., Cabrera, J., Ghosh, S., Jiang, Y., Yan, J., Lee, J., Makam, S., et al. (2018). Enhancer variants reveal a conserved transcription factor network governed by PU.1 during osteoclast differentiation. Bone Res. *6*, 8.

Charles, J.F., and Aliprantis, A.O. (2014). Osteoclasts: more than 'bone eaters'. Trends Mol. Med. *20*, 449–459.

Chiang, C.M. (2009). Brd4 engagement from chromatin targeting to transcriptional regulation: selective contact with acetylated histone H3 and H4. F1000 Biol. Rep. *1*, 98.

Collin-Osdoby, P., and Osdoby, P. (2012). RANKL-mediated osteoclast formation from murine RAW 264.7 cells. Methods Mol. Biol. *816*, 187–202.

Collin-Osdoby, P., Yu, X., Zheng, H., and Osdoby, P. (2003). RANKL-mediated osteoclast formation from murine RAW 264.7 cells. Methods Mol. Med. *80*, 153–166.

Davidson, R.K., Himes, E.R., Takigawa, S., Chen, A., Horn, M.R., Meijome, T., Wallace, J.M., Kacena, M.A., Yokota, H., Nguyen, A.V., and Li, J. (2020). The loss of STAT3 in mature osteoclasts has detrimental effects on bone structure. PLoS One *15*, e0236891.

Edwards, C.M., Zhuang, J., and Mundy, G.R. (2008). The pathogenesis of the bone disease of multiple myeloma. Bone *42*, 1007–1013.

Fernandez-Alonso, R., Davidson, L., Hukelmann, J., Zengerle, M., Prescott, A.R., Lamond, A., Ciulli, A., Sapkota, G.P., and Findlay, G.M. (2017). Brd4-Brd2 isoform switching coordinates pluripotent exit and Smad2-dependent lineage specification. EMBO Rep. *18*, 1108–1122.

Franzoso, G., Carlson, L., Xing, L., Poljak, L., Shores, E.W., Brown, K.D., Leonardi, A., Tran, T., Boyce, B.F., and Siebenlist, U. (1997).

Requirement for NF-kappaB in osteoclast and B-cell development. Genes Dev. *11*, 3482–3496.

Hnisz, D., Abraham, B.J., Lee, T.I., Lau, A., Saint-Andre, V., Sigova, A.A., Hoke, H.A., and Young, R.A. (2013). Super-enhancers in the control of cell identity and disease. Cell *155*, 934–947.

Hsu, H., Lacey, D.L., Dunstan, C.R., Solovyev, I., Colombero, A., Timms, E., Tan, H.L., Elliott, G., Kelley, M.J., Sarosi, I., et al. (1999). Tumor necrosis factor receptor family member RANK mediates osteoclast differentiation and activation induced by osteoprotegerin ligand. Proc. Natl. Acad. Sci. U S A *96*, 3540–3545.

Hu, M., Bassett, J.H., Danks, L., Howell, P.G., Xu, K., Spanoudakis, E., Kotsianidis, I., Boyde, A., Williams, G.R., Horwood, N., et al. (2011). Activated invariant NKT cells regulate osteoclast development and function. J. Immunol. *186*, 2910–2917.

Huijbregts, L., Petersen, M.B.K., Berthault, C., Hansson, M., Aiello, V., Rachdi, L., Grapin-Botton, A., Honore, C., and Scharfmann, R. (2019). Bromodomain and extra terminal protein inhibitors promote pancreatic endocrine cell fate. Diabetes *68*, 761–773.

Izawa, N., Kurotaki, D., Nomura, S., Fujita, T., Omata, Y., Yasui, T., Hirose, J., Matsumoto, T., Saito, T., Kadono, Y., et al. (2019). Cooperation of PU.1 with IRF8 and NFATc1 defines chromatin landscapes during RANKL-induced osteoclastogenesis. J. Bone Miner. Res. *34*, 1143–1154.

Kim, K., Kim, J.H., Lee, J., Jin, H.M., Kook, H., Kim, K.K., Lee, S.Y., and Kim, N. (2007). MafB negatively regulates RANKL-mediated osteoclast differentiation. Blood *109*, 3253–3259.

Kukita, T., Wada, N., Kukita, A., Kakimoto, T., Sandra, F., Toh, K., Nagata, K., Iijima, T., Horiuchi, M., Matsusaki, H., et al. (2004). RANKL-induced DC-STAMP is essential for osteoclastogenesis. J. Exp. Med. *200*, 941–946.

Kurotaki, D., Yoshida, H., and Tamura, T. (2020). Epigenetic and transcriptional regulation of osteoclast differentiation. Bone *138*, 115471.

Lamoureux, F., Baud'huin, M., Rodriguez Calleja, L., Jacques, C., Berreur, M., Redini, F., Lecanda, F., Bradner, J.E., Heymann, D., and Ory, B. (2014). Selective inhibition of BET bromodomain epigenetic signalling interferes with the bone-associated tumour vicious cycle. Nat. Commun. *5*, 3511.

Langlais, D., Barreiro, L.B., and Gros, P. (2016). The macrophage IRF8/IRF1 regulome is required for protection against infections and is associated with chronic inflammation. J. Exp. Med. *213*, 585–603.

Lee, J.E., Park, Y.K., Park, S., Jang, Y., Waring, N., Dey, A., Ozato, K., Lai, B., Peng, W., and Ge, K. (2017). Brd4 binds to active enhancers to control cell identity gene induction in adipogenesis and myogenesis. Nat. Commun. *8*, 2217.

Le Pape, F., Vargas, G., and Clezardin, P. (2016). The role of osteoclasts in breast cancer bone metastasis. J. Bone Oncol. *5*, 93–95.

LeRoy, G., Rickards, B., and Flint, S.J. (2008). The double bromodomain proteins Brd2 and Brd3 couple histone acetylation to transcription. Mol. Cell *30*, 51–60.

Loven, J., Hoke, H.A., Lin, C.Y., Lau, A., Orlando, D.A., Vakoc, C.R., Bradner, J.E., Lee, T.I., and Young, R.A. (2013). Selective inhibition of tumor oncogenes by disruption of super-enhancers. Cell *153*, 320–334.

Miyauchi, Y., Ninomiya, K., Miyamoto, H., Sakamoto, A., Iwasaki, R., Hoshi, H., Miyamoto, K., Hao, W., Yoshida, S., Morioka, H., et al. (2010). The Blimp1-Bcl6 axis is critical to regulate osteoclast differentiation and bone homeostasis. J. Exp. Med. *207*, 751–762.

Nishikawa, K., Nakashima, T., Hayashi, M., Fukunaga, T., Kato, S., Kodama, T., Takahashi, S., Calame, K., and Takayanagi, H. (2010). Blimp1-mediated repression of negative regulators is required for osteoclast differentiation. Proc. Natl. Acad. Sci. U S A *107*, 3117–3122.

Park-Min, K.H., Lim, E., Lee, M.J., Park, S.H., Giannopoulou, E., Yarilina, A., van der Meulen, M., Zhao, B., Smithers, N., Witherington, J., et al. (2014). Inhibition of osteoclastogenesis and inflammatory bone resorption by targeting BET proteins and epigenetic regulation. Nat. Commun. *5*, 5418.

Rahman, S., Sowa, M.E., Ottinger, M., Smith, J.A., Shi, Y., Harper, J.W., and Howley, P.M. (2011). The Brd4 extraterminal domain confers transcription activation independent of pTEFb by recruiting multiple proteins, including NSD3. Mol. Cell Biol. *31*, 2641–2652.

Raschke, W.C., Baird, S., Ralph, P., and Nakoinz, I. (1978). Functional macrophage cell lines transformed by Abelson leukemia virus. Cell *15*, 261–267.

Roe, J.S., Mercan, F., Rivera, K., Pappin, D.J., and Vakoc, C.R. (2015). BET bromodomain inhibition Suppresses the function of hematopoietic transcription factors in acute myeloid leukemia. Mol. Cell *58*, 1028–1039.

Soysa, N.S., Alles, N., Aoki, K., and Ohya, K. (2012). Osteoclast formation and differentiation: an overview. J. Med. Dent. Sci. *59*, 65–74.

Sundaram, K., Nishimura, R., Senn, J., Youssef, R.F., London, S.D., and Reddy, S.V. (2007). RANK ligand signaling modulates the matrix metalloproteinase-9 gene expression during osteoclast differentiation. Exp. Cell Res. *313*, 168–178.

Takayanagi, H., Kim, S., Koga, T., Nishina, H., Isshiki, M., Yoshida, H., Saiura, A., Isobe, M., Yokochi, T., Inoue, J., et al. (2002). Induction and activation of the transcription factor NFATc1 (NFAT2) integrate RANKL signaling in terminal differentiation of osteoclasts. Dev. Cell *3*, 889–901.

Teitelbaum, S.L. (2000). Bone resorption by osteoclasts. Science *289*, 1504–1508.

Troen, B.R. (2006). The regulation of cathepsin K gene expression. Ann. N. Y Acad. Sci. *1068*, 165–172.

Wagner, E.F. (2002). Functions of AP1 (Fos/Jun) in bone development. Ann. Rheum. Dis. *61*, 40–42.

Whyte, W.A., Orlando, D.A., Hnisz, D., Abraham, B.J., Lin, C.Y., Kagey, M.H., Rahl, P.B., Lee, T.I., and Young, R.A. (2013). Master transcription factors and mediator establish super-enhancers at key cell identity genes. Cell *153*, 307–319.

Wu, H., Xu, G., and Li, Y.P. (2009). Atp6v0d2 is an essential component of the osteoclast-specific proton pump that mediates extracellular acidification in bone resorption. J. Bone Miner. Res. *24*, 871–885.

Yang, M., Birnbaum, M.J., MacKay, C.A., Mason-Savas, A., Thompson, B., and Odgren, P.R. (2008). Osteoclast stimulatory transmembrane protein (OC-STAMP), a novel protein induced by RANKL that promotes osteoclast differentiation. J. Cell Physiol. *215*, 497–505.

Yu, C., Niu, X., Jin, F., Liu, Z., Jin, C., and Lai, L. (2016). Structure-based inhibitor design for the intrinsically disordered protein c-myc. Sci. Rep. *6*, 22298.

Zhao, B., Takami, M., Yamada, A., Wang, X., Koga, T., Hu, X., Tamura, T., Ozato, K., Choi, Y., Ivashkiv, L.B., et al. (2009). Interferon regulatory factor-8 regulates bone metabolism by suppressing osteoclastogenesis. Nat. Med. *15*, 1066–1071.

iScience, Volume *24*

Supplemental Information

Brd2/4 and Myc regulate alternative cell lineage programmes during early osteoclast differentiation in vitro

Valentina S. Caputo, Nikolaos Trasanidis, Xiaolin Xiao, Mark E. Robinson, Alexia Katsarou, Kanagaraju Ponnusamy, Rab K. Prinjha, Nicholas Smithers, Aristeidis Chaidos, Holger W. Auner, and Anastasios Karadimitris

Supplementary File

Brd2/4 and Myc regulate alternative cell lineage programmes during early osteoclast development in vitro

Valentina S Caputo[1]*, Nikolaos Trasanidis[1]*, Xiaolin Xiao[1]*, Mark E Robinson[1], Alexia Katsarou[1,2], Kanagaraju Ponnusamy[1], Rab K Prinjha[3], Nicholas Smithers[3], Aristeidis Chaidos[1,2], Holger W Auner[1,2] and Anastasios Karadimitris[1,2†]

[1]Hugh & Josseline Langmuir Centre for Myeloma Research, Centre for Haematology, Department of Immunology and Inflammation, Imperial College London, London, UK
[2]Department of Haematology, Hammersmith Hospital, Imperial College Healthcare NHS Foundation Trust, London, UK
[3]Medicines Research Centre, GlaxoSmithKline, Stevenage, United Kingdom

Transparent methods

Cell culture

RAW264.7 cells were maintained in DMEM media (Sigma) containing 10% FBS (Life technologies), 1000U/ml penicillin/streptomycin (Sigma). HEK293T cells were cultured in DMEM media (Sigma) supplemented with 10% FBS (Sigma). Cells were grown at 37^0C under 5% CO2.

Primary osteoclast and Osteoclast progenitors

Bone marrow cells (BM) were harvested from murine tibias and femurs of C57BL/6 male mice, washed with PBS. Red cells were lysed with RCL (eBioscience) and washed again with PBS. To obtain osteoclast progenitors (OCP), BM cells were stained with anti-CD11b PerCP, -CD3e FITC, -CD115 PE, -B220 FITC and -cKIT APC (from BD Pharmingen) using standard protocols and flow-sorted as described in (Hu et al., 2011) using a BD FACSAriaII flow-sorter.

BM cells were cultured in α-MEM (Life technologies) containing 10% FBS (Life technologies) and 1% penicillin-streptomycin (Sigma) and 20 ng/ml M-CSF (Preprotech) overnight at a density of 1×10^6 cells/ml. Non-adherent BM cells were harvested the next day as source of primary osteoclasts.

Osteoclast assays

Osteoclast progenitors (OCP) and non-adherent BM cells were seeded into 24/48 or 96 well/plates in complete media with 20 ng/ml M-CSF (Preprotech) and 50 ng/ml RANKL (Preprotech) at a density of 1×10^6 cells/ml (1ml per 24 w, 500ul /48w and 200 ul/ 96 well). RAW264.7 cell were seeded at a density of 1×10^6 cells/ml (1ml per 24 w, 500ul /48w and 200 ul/ 96 well) and cultured in presence of 50ng/ml RANKL (Preprotec)

For all the cultures, after 2-3 days of culture, media was changed. After 6-7 dyas the cells were fixed and stained for TRAP activity using the TRAP assay kit (Sigma).

Multinucleated cells with 3 or more nuclei were counted as TRAP+ cells. Images were acquired using EVOS cell imagine system (Thermofisher) (Ersek et al., 2015).

shRNA constructs and lentivirus production

ShRNA oligoes were phosphorylated and annealed and cloned, using the AgeI and EcoRI sites into a modified lentiviral pLKO.1 vector (Sigma), in which the puromycin gene had been replaced with eGFP. A scrambled shRNA was used as control. The following oligoes were used for the shRNA cloning:

-*Sh Mm MYC Forward primer*: 5'-
CCGGGACTCCGTACAGCCCTATTTCCTCGAGGAAATAGGGCTGTACGGAGTCTTTTTG-3'
-*Sh Mm MYC Reverse primer*: 5'-
AATTCAAAAAGACTCCGTACAGCCCTATTTCCTCGAGGAAATAGGGCTGTACGGAGTC
-3'

Recombinant lentiviruses were produced by co-transfecting the pLKO.1-GFPshRNA plasmid with helper plasmids (pRSV.REV, pMDLgpRRE and pMD2.VSVG) into HEK293T cells using the calcium phosphate method. After 24h of transfection, the medium was replaced. Viral supernatant was collected at 48h and 72h post transfection. Lentiviruses were concentrated by ultracentrifugation at 23000rpm for 1.5h at 4^0C. Cells were transduced in the presence of polybrene (8µg/ml final concentration; Sigma). Two days post-transduction, GFP positive cells were FACS-sorted using a BD FACSAriaII flow-sorter.

Reverse transcription PCR and qRT-PCR

Total RNA was isolated from cultured cells using the ReliaPrep RNA cell Miniprep System (Promega). cDNA was synthesized with RevertAid cDNA synthesis kit (Thermoscientific). qRT-PCR was performed with Taqman probes (Applied Biosystems) using an AB StepOne Plus Real-Time PCR (Applied Biosystems). Gene expression was normalized to the expression of *HPRT* housekeeping gene using the ΔCt method. Taqman probes: *Myc* (Mm00487804_m1), *Brd2* (Mm01271171_s1), *Brd4* (Mm00480394_m1), *Nfatc1* (Mm00479445_m1), *Irf8* (Mm00492567_m1), *Ocstamp* (Mm00512445_m1), *Dcstam*p (Mm04209236_m1) and *Hprt* (Mm00446968_m1).

RNA-seq

Total RNA was isolated from RAW264.7 cells at 0, 4, 14 and 24h after RANKL, RANKL/I-BET, I-BET- treatment (two independent experiments per time point and condition) using the Nucleospin RNA kit (Macherey-Nagel). RNA quantity was determined with Qubit using the Qubit RNA Assay kit (Life Technologies) and RNA quality was assessed on the Bioanalyser using the RNA pico kit (Agilent). Libraries were prepared using the NEBNext poly(A) mRNA Magnetic Isolation Module and the NEBNext Ultra RNA Library Prep kit for Illumina (NEB), following manufacturer's instructions. Library quantity was determined using the Qubit High Sensitivity DNA kit (Life Technologies) and library size was determined using the Bioanalyser High Sensitivity DNA kit (Agilent). Libraries were quantified using the Universal Library Quantification Kit for Illumina (Kapa Biosystems) and run on AB StepOne Plus Real-Time PCR (Applied Biosystems). Libraries were diluted to 2nM and sequenced using the Illumina HiSeq 2500 platform to obtain paired-end 100bp reads. Two replicate per time point and treatment were made.

Chromatin immunoprecipitation

Chromatin immunoprecipitation (ChIP)-qPCR was performed as described in (Caputo et al., 2013). Specifically, after 4 h treatment RAW264.7 cells were washed with PBS and crosslinked with 1% formaldehyde (SIGMA) for 15 min at room temperature.

Crosslinking was stopped by the addition of glycine (1.25M) to a final 125 mM concentration. Subsequently, the cells were washed 3 times with ice cold PBS and pelleted at 300g. The crosslinked cells were lysed for 20 min on ice, and the nuclei were sonicated for 5 times for 5 min each time using a 30sec/30 sec off cycles, at 4^0C, under high intensity in a Bioruptor UCD-200 (Diagenode).
Sonicated fragments ranged 500-300bp in length. The sonicated chromatin was diluted at least ten times with ChIP dilution buffer (0,01%SDS, 1,1% Triton X-100, 1,2mM EDTA, 16,7mM Tris-HCL pH 8, 167mM NaCl) with freshly added proteinase inhibitors (Sigma). To avoid unspecific binding, the diluted chromatin was pre-cleared for 1h at 4^0 C with magnetic beads (Dynabeads Protein A+G form Invitrogen). 3-5ug of antibody was added to pre-cleared chromatin aliquots and incubated overnight at 4^0C on a rotating wheel.
Immunoprecipitation was achieved by addition of protein A+G (50% each) magnetic beads and incubating for 2-4h at 4^0C on a rotating wheel. Immunoprecipitated complexes were washed for 5 min with salt buffer (0.1% SDS, 1% Triton X-100, 2mM EDTA, 20mM Tris-HCl pH 8, 150mM NaCl), high salt buffer (0.1% SDS, 1% Triton X-100, 2mM EDTA, 20mM Tris-HCl pH 8, 500mM NaCl), LiCl buffer (0,25M LiCl, 1 % IGEPAL, 1% sodium deoxicolate, 1mM EDTA, 10mM Tris-HCl pH 8) and TE. All the washed were perform twice at 4^0C on a rotating wheel.
Elution and un-crosslinking were achieved by incubating the immoprecipitated complexes with 150μl elution buffer (50mM Tris-HCl pH 8, 50mM NaCl, 1mM EDTA and freshly added 1% SDS and 20mg/ml of RNaseA) at 65^0C overnight and again a second time for 30 min. Eluted complexes were treated with proteinase K (Thermoscientific) for 45 min at 45^0C.
DNA was purified by phenol extraction and ethanol DNA precipitation. Q-PCR was performed using SYBR Select Master Mix (Lifetechnologies) on a StepOne Plus Real-Time PCR (Applied Biosystems). Enrichment of the target sequence was assessed against INP DNA and IgG control (C1111), cMYC (sc764), Max (SC197), Brd2 (Bethyl A302-582A). Brd3 (Bethyl A302-368A) and Brd4 (Bethyl A301-985150), H3K27ac (ab4729).

ChIP-seq
Treated and untreated cells were cultured using DMEM medium.10^7 cells per ChIP were cross-linked with 1% formaldehyde for 15min. Chromatin immunoprecipitation was performed as described above. The ChIP DNA was purified with AMPure beads (Beckman). ChIP and input DNA libraries were prepared using the NEBNext ChIP-seq Library Prep Master Mix for Illumina (NEB) following manufacturer's protocols. The quantity was determined using the Qubit High Sensitivity DNA kit (Life Technologies) and library size was determined using the Bioanalyser High Sensitivity DNA kit (Agilent). Libraries concentration was quantified using the Universal Library Quantification Kit for Illumina (Kapa Biosystems) using a AB StepOne Plus Real-Time PCR (Applied Biosystems). Libraries were diluted to a final concentration of 2nM and sequenced at the MRC Imperial facility using the Illumina HiSeq 2500 platform to obtain single-end 50bp reads.

ATAC-seq
ATAC seq was performed as described in (Buenrostro et al., 2015). Briefly, 50.000 cells were collected and washed at 500g at 4^0C for 5 min with PBS. The cell pellet was resuspended in ATAC lysis buffer and immediately spun for 10 min at 500g at 4^0C. The nuclei were then subjected to Tn reaction for 30 min at 37^0C; the reaction was terminated and the DNA purified immediately using a MinElute Kit (Qiagen). The purified DNA was amplified with NEBNext High-Fidelity 2x PCR Master Mix (NEB). The PCR amplified product was cleaned with AMPure beads (Beckman). The quality of the libraries was assessed with the Bioanalyser High Sensitivity DNA kit (Agilent). The library was quantified with using the Universal Library Quantification Kit for

Illumina (Kapa Biosystems) on a StepOne Plus Real-Time PCR (Applied Biosystems). The libraries were sequenced at the Genomics Facility at MRC/LIMS of ICL using the Illumina HiSeq 2500 platform to obtain paired-end 100bp reads.

Bioinformatic analysis

ChIP-Seq

ChIP-Seq normalisation and analysis

Bowtie 2.3.4.1 (64 bit) was used to map ChIP-Seq reads to the mm10 mouse reference genome using default parameters and samtools 1.2 was used to convert SAM files, sorting and indexing BAM files. The Picard package was used to remove duplicated reads and the reads mapped on unknown and random chromosomes, in BAM files. MACS2 (v2.1) was used for peaks calling for each sample (Brd, Myc, Max, and H3K27ac) against their corresponding control input DNA. Significant peaks were obtained by applying an appropriate q-value cutoff (Brds, broad peaks calling at q<0.05; Myc, narrow peaks calling at q<0.1; Max, narrow peaks calling at q<0.01; H3K27ac, broad peaks calling at q<0.01). The significant ChIP-Seq peaks from MACS2 were annotated using the ChIPpeakAnno (Zhu, 2013; Zhu et al., 2010) and Homer package against the built-in mm10 mouse genome with the default settings. The R/Bioconductor package Diffbind (Ross-Innes et al., 2012) was used to obtain differential binding sites (DBS) across different conditions (R, RI, I, S) for samples (Brd and H3K27ac). For this purpose, three pseudo-replicates per ChIPseq sample were obtained by down-sampling to the minimum read depth; only peaks detected consistently in 2 out of 3 pseudo-replicates were used for DBS analysis. Furthermore, bedops tools were used on Brd2 and Brd4 DBS to generate Venn diagrams (**Figure 2E**) for different comparisons. The ChIPpeakAnno package was also used to annotate all significant DBS (FDR<0.05) and identify overlaps between H3K27ac annotated regions with the Brds significant DBS (FDR<0.05).

In addition, the Homer tools *findMotifsGenome* function was used to perform known and de-novo motifs analysis against the built-in mm10 mouse genome for the significant ChIP-Seq peaks (Figure 4E).

Super-enhancer calling

To identify the list of super-enhancers (SE) for each condition (S,R,RI,I), the significantly enriched H3K27ac peaks obtained from MACS2 were analysed further using the Ranking Of Super Enhancers (ROSE) package (Whyte et al., 2013) (Loven et al., 2013) (**Figure 3D**). Correspondingly, the SE regions were annotated using the ChIPpeakAnno package

Genomic regions visualization

The IGV Genome Browser was used for genomic regions visualization. The DeepTools toolkit (Ramirez et al., 2016) was used to generate heatmaps and metagene plots of the Brd2,3,4 signal over the significant DBS(FDR<0.05: -10kb - +10kb region around the peak center) (Figure 2D), and the choromatin analysis and exploration (ChAsE) (Younesy et al., 2016) tool was applied to visualize Input, Myc and Max ChIPseq signals (±2 kb around the peak center) (Figure 4C).

RNA-Seq

The pair-end reads from the RNA-Seq experiments for all the 4 conditions (S/R/Ri/I) across the different time points (0, 4, 14 and 24h) were aligned to the GRCm38 (mm10) reference genome by STAR (version 2.5.3a) with 10,000 as the max number of different alignments per read to consider (--alignTranscriptsPerReadNmax 100000). To ensure the large reads files to be processed smoothly, the limits settings in STAR were increased (--limitGenomeGenerateRAM 20000000000). The “Rsubread” (version 1.24.2) R/Bioconductor package was used to obtain the raw read counts per

library using the GRCm38 reference genome. The "DESeq2" (version 1.16.1) (Love et al., 2014) R/Bioconductor package was used for normalising the counts and implementing the Differential Gene Expression (DGE) analysis across timepoints and treatments. The R package "pheatmap" was used to draw the initial clustered heatmaps for the selected differential expressed genes (|lfc|>0.8 and padj<0.05) of each contrast across conditions. The correlation was computed as the dissimilarity between the selected DEGs in order to capture their expression changes across all the time points (h0, h4, h14 and h24). Then an R package for performing Weighted Gene Co-expression Network Analysis (WGCNA) (Langfelder and Horvath, 2008) (Zhang and Horvath, 2005) was used to find clusters (modules) of highly correlated genes based on the dendrogram tree of the initial clustered heatmaps. Comparative PCA and MA plots were generated using the PCA and maPlot functions in R. Gene set enrichment analysis (enriched GO, pathways, etc.) was performed for the clusters using enrichR (Chen et al., 2013; Kuleshov et al., 2016)

ATAC-Seq

ATAC-Seq reads were trimmed using TrimGallore (--paired -q 30 --nextera) and aligned against the mm10 mouse reference genome using Bowtie 2.3.4.1(-X 2000). SAM files conversion and BAM files sorting and indexing were performed using samtools. The picard and samtools packages were used to remove duplicate reads and reads mapped on chrUn, chr_random and chrM chromosomes, respectively. Peak calling was performed using MACS2 (*-B –nomodel –call-summits -q 0.01*) and deepTools functions were used to obtain pileup tracks. The ENCODE backlisted regions for mm10 were removed using bedtools (https://www.nature.com/articles/s41598-019-45839-z). The pyDNAse (Wellington) algorithm was used for TF footprinting; the genome-wide Tn5 cut site tracks (bigwig), the Tn5 signal per TF and the predicted TF biding sites were obtained using the default package parameters. TF motif calling on significant footprints (cutoff=20) was performed using Homer against HOCOMOCOv11 core database. To remove redundant and overlapping motifs, motif similarity was determined using TomTom from the MEME suite, and grouped into highly similar motif-classes (q<0.01). To predict the most likely candidate TF responsible for each footprint, all TF within the motif-class detected in the footprint region were ranked by an overall score of expression level and change in osteoclastogenesis ($-\log_{10}(padj)*|\log_2FC|*\log_2(RPKM+1)$), and highest scoring TF selected. Only TF genes were considered for GRN visualization, as plotted with the igraph package.

Integrative Analysis

Integrative analysis on ChIPseq and RNAseq data

The Beta package (Binding and Expression Target Analysis) was applied to integrate the Myc ChIP-Seq data with Differential Expressed (DE) genes from RNA-Seq data across different time points (4, 14, and 24 h). Also, ChIP-Seq data (Brd, and H3K27ac) and their differential binding sites (Brd DBS and H3K27ac DBS) were annotated to the closest differentially expressed gene.

Published datasets usage

The previously published RNA-Seq data (SRP096890) and Irf8/Pu.1 ChIPseq were used for additional comparisons and validation (Langlais et al., 2016).

Data availability

All data are accessible from Gene Expression Omnibus database (Acc. Number: GSE160840).

Supplementary Figure Legends

Figure S1, Related to Figure 1. Transcriptional and cellular responses of RAW264.7 and primary precursor cells to RANKL and I-BET151. (**A**) Flow cytometry strategy for identification and isolation of osteoclast progenitors. (**B**) Top: TRAP staining of RAW264.7, bone-marrow OC precursors (BM OCP) and purified osteoclast progenitors upon treatment with RANKL (50ng/ml) and RANKL/I-BET151 (500nM); n=2-6 independent experiments in triplicates. Bottom: quantification of TRAP+ cells/well per condition. Results represent mean and SEM t test; ***, p=0.0001; ****, p< 0.0001 (**C**) Correlation matrix comparing overlap between significantly up- and down- regulated genes identified in RAW264.7 cells 24h post RANKL-induction with those of primary OC at 48h (WT Myc R vs S, (Bae et al., 2017)). Color key represents corresponding odds ratios. (**D**) Time course qPCR profiling of *Myc, Irf8, Dcstamp and Ocstamp* expression in murine primary bone marrow-derived pre-osteoclast cells; (n=3 mice). Results represent mean and SEM (One-way ANOVA: **, p<0.01; ***, p<0.001; ****, p<0.0001). (**E**) RNA-seq analysis in RAW264.7 cells. Top: PCA analysis of differentially expressed genes (12 clusters derived from R vs S analysis) across time points (4,14,24hr) and comparisons (RvsS, IvsS, RvsI and RvsRI); bottom: MA plot of 12 gene clusters across comparisons at 24h after treatments.

Figure S2. Related to Figure 1. Dynamic transcriptional alterations during early osteoclast development in response to RANKL and I-BET151. (A) Time course profiling of *Nfatc1* expression after RANKL-, I-BET151- or RANKL/I-BET151 treatment (left, qRT-PCR; right, RNAseq); values were normalized to time 0. (**B**) Enrichment analysis (left: ChEA, right: Mouse Gene Atlas) on 156 genes included in Cluster 7 (displayed in **Fig1B**). (**C**) Heatmap illustration of pairwise treatment comparisons (R vs S, I vs. S, RI vs R) at 0,4,14 and 24h, as analysed by RNA-Seq in RAW 264.7 cells. **(D)** qPCR profiling of *Myc, Irf8, Dcstamp and Ocstamp* expression in murine primary bone marrow-derived pre-osteoclast cells 4h after no treatment (S), treatment with RANKL (R), RANKL/I-BET151 (RI) or I-BET151; (n=3 mice). Results represent mean and SEM (One-way ANOVA: *, p<0.05; **, p<0.01)

Figure S3, related to Figure 2. Time course profiling of BET proteins expression after RANKL-, IBET151- or RANKL/I-BET151 treatments. (**A**) RNA-Seq and (**B**) qRT-PCR time course experiments.

Figure S4, related to Figure 3. Functional annotation of transcriptional responses associated with Brd2,4 chromatin binding. (**A**) Line plots indicating expression patters of all predicted target genes with increased associated Brd2,4 binding in RANKL treated cells. (**B**) IGV snapshot illustrating the Brd4 and H3K27ac enrichment, along with the identified super-enhancer, across S,R,I conditions on the *Fos* genetic locus. Overrepresentation analysis of differentially expressed genes at 4 (**C**) and 14h (**D**) associated with super-enhancer (SE) and typical enhancer (E) regulation**.** EnrichR analysis using databases: ChEA, KEGG pathways, Gene ontology, WIKI pathways and NCI nature.

Figure S5, **related to Figure 4. The gene regulatory network of the early developmental events during osteoclast development.** (**A**) Genome-wide Tn5

footprinting profiles for each transcription factor. (**B**) Time course profiling of *Myc* expression at 0, 4, 14 and 24h after RANKL, I-BET151 or RANKL/I-BET151 treatment using qRT-PCR and RNA-seq (**C**). Individual regulatory modules for indicated TF. Arrow width indicates footprint score for originating TF at target gene promoter/enhancer, colour indicates direction of expression change for originating TF. Node size indicates strength of expression change ($-\log_{10}(padj)*|\log_2 FC|$) and colour indicates direction of change at 14h post-RANKL treatment, (Red=upregulated and blue=downregulated).

Figure S6, **related to Figure 4. Phenotypic and epigenomic characterization of *Myc* at the early stages of osteoclast development.** *Myc* mRNA, TRAP OC assay and TRAP+ OC numbers/well after treatment shRNA-mediated *Myc* knock-down (shMyc) in RAW 274.7 cells (**A**) or (**B**) their treatment with the Myc-Max inhibitor 10058-F4 (F4 50mM). *Myc* expression is shown relative to *Hprt* and scrbl or un-treated cells, respectively; n=3-5 independent experiments with triplicate technical replicates. (**C**) The epigenomic landscape of the 560 Myc-bound regions in developing osteoclasts. Violin plots displaying the relative enrichment ($\log_2$ scale) of H3K27ac and Brd2-4 on the Myc-bound regions across S, R, RI and I conditions. (**D)** EnrichR overrepresentation analysis of differentially expressed genes (14h post RANKL-induction) with associated Myc and Brd2,4 binding sites. EnrichR analysis (ChEA, KEGG pathways, Gene ontology, WIKI pathways and NCI nature). *, $p<0.05$; ***, $p<0.001$; ****, $p<0.0001$.

References

Azuma, Y., Kaji, K., Katogi, R., Takeshita, S., and Kudo, A. (2000). Tumor necrosis factor-alpha induces differentiation of and bone resorption by osteoclasts. J Biol Chem *275*, 4858-4864.

Bae, S., Lee, M. J., Mun, S. H., Giannopoulou, E. G., Yong-Gonzalez, V., Cross, J. R., Murata, K., Giguere, V., van der Meulen, M., and Park-Min, K. H. (2017). MYC-dependent oxidative metabolism regulates osteoclastogenesis via nuclear receptor ERRalpha. J Clin Invest *127*, 2555-2568.

Baud'huin, M., Lamoureux, F., Jacques, C., Rodriguez Calleja, L., Quillard, T., Charrier, C., Amiaud, J., Berreur, M., Brounais-LeRoyer, B., Owen, R.*, et al.* (2017). Inhibition of BET proteins and epigenetic signaling as a potential treatment for osteoporosis. Bone *94*, 10-21.

Boyce, B. F. (2013). Advances in the regulation of osteoclasts and osteoclast functions. J Dent Res *92*, 860-867.

Buenrostro, J. D., Wu, B., Chang, H. Y., and Greenleaf, W. J. (2015). ATAC-seq: A Method for Assaying Chromatin Accessibility Genome-Wide. Curr Protoc Mol Biol *109*, 21 29 21-21 29 29.

Caputo, V. S., Costa, J. R., Makarona, K., Georgiou, E., Layton, D. M., Roberts, I., and Karadimitris, A. (2013). Mechanism of Polycomb recruitment to CpG islands revealed by inherited disease-associated mutation. Hum Mol Genet *22*, 3187-3194.

Carey, H. A., Hildreth, B. E., 3rd, Geisler, J. A., Nickel, M. C., Cabrera, J., Ghosh, S., Jiang, Y., Yan, J., Lee, J., Makam, S.*, et al.* (2018). Enhancer variants reveal a conserved transcription factor network governed by PU.1 during osteoclast differentiation. Bone Res *6*, 8.

Charles, J. F., and Aliprantis, A. O. (2014). Osteoclasts: more than 'bone eaters'. Trends Mol Med *20*, 449-459.

Chen, E. Y., Tan, C. M., Kou, Y., Duan, Q., Wang, Z., Meirelles, G. V., Clark, N. R., and Ma'ayan, A. (2013). Enrichr: interactive and collaborative HTML5 gene list enrichment analysis tool. BMC Bioinformatics *14*, 128.

Chiang, C. M. (2009). Brd4 engagement from chromatin targeting to transcriptional regulation: selective contact with acetylated histone H3 and H4. F1000 Biol Rep *1*, 98.

Collin-Osdoby, P., and Osdoby, P. (2012). RANKL-mediated osteoclast formation from murine RAW 264.7 cells. Methods Mol Biol *816*, 187-202.

Collin-Osdoby, P., Yu, X., Zheng, H., and Osdoby, P. (2003). RANKL-mediated osteoclast formation from murine RAW 264.7 cells. Methods Mol Med *80*, 153-166.
Davidson, R. K., Himes, E. R., Takigawa, S., Chen, A., Horn, M. R., Meijome, T., Wallace, J. M., Kacena, M. A., Yokota, H., Nguyen, A. V., and Li, J. (2020). The loss of STAT3 in mature osteoclasts has detrimental effects on bone structure. PLoS One *15*, e0236891.

Edwards, C. M., Zhuang, J., and Mundy, G. R. (2008). The pathogenesis of the bone disease of multiple myeloma. Bone *42*, 1007-1013.

Ersek, A., Xu, K., Antonopoulos, A., Butters, T. D., Santo, A. E., Vattakuzhi, Y., Williams, L. M., Goudevenou, K., Danks, L., Freidin, A.*, et al.* (2015). Glycosphingolipid synthesis inhibition limits osteoclast activation and myeloma bone disease. J Clin Invest *125*, 2279-2292.

Fernandez-Alonso, R., Davidson, L., Hukelmann, J., Zengerle, M., Prescott, A. R., Lamond, A., Ciulli, A., Sapkota, G. P., and Findlay, G. M. (2017). Brd4-Brd2 isoform switching coordinates pluripotent exit and Smad2-dependent lineage specification. EMBO Rep *18*, 1108-1122.

Franzoso, G., Carlson, L., Xing, L., Poljak, L., Shores, E. W., Brown, K. D., Leonardi, A., Tran, T., Boyce, B. F., and Siebenlist, U. (1997). Requirement for NF-kappaB in osteoclast and B-cell development. Genes Dev *11*, 3482-3496.

Hnisz, D., Abraham, B. J., Lee, T. I., Lau, A., Saint-Andre, V., Sigova, A. A., Hoke, H. A., and Young, R. A. (2013). Super-enhancers in the control of cell identity and disease. Cell *155*, 934-947.

Hsu, H., Lacey, D. L., Dunstan, C. R., Solovyev, I., Colombero, A., Timms, E., Tan, H. L., Elliott, G., Kelley, M. J., Sarosi, I.*, et al.* (1999). Tumor necrosis factor receptor family member RANK mediates osteoclast differentiation and activation induced by osteoprotegerin ligand. Proc Natl Acad Sci U S A *96*, 3540-3545.

Hu, M., Bassett, J. H., Danks, L., Howell, P. G., Xu, K., Spanoudakis, E., Kotsianidis, I., Boyde, A., Williams, G. R., Horwood, N.*, et al.* (2011). Activated invariant NKT cells regulate osteoclast development and function. J Immunol *186*, 2910-2917.

Huijbregts, L., Petersen, M. B. K., Berthault, C., Hansson, M., Aiello, V., Rachdi, L., Grapin-Botton, A., Honore, C., and Scharfmann, R. (2019). Bromodomain and Extra Terminal Protein Inhibitors Promote Pancreatic Endocrine Cell Fate. Diabetes *68*, 761-773.

Izawa, N., Kurotaki, D., Nomura, S., Fujita, T., Omata, Y., Yasui, T., Hirose, J., Matsumoto, T., Saito, T., Kadono, Y.*, et al.* (2019). Cooperation of PU.1 With IRF8 and NFATc1 Defines Chromatin Landscapes During RANKL-Induced Osteoclastogenesis. J Bone Miner Res *34*, 1143-1154.

Kim, K., Kim, J. H., Lee, J., Jin, H. M., Kook, H., Kim, K. K., Lee, S. Y., and Kim, N. (2007). MafB negatively regulates RANKL-mediated osteoclast differentiation. Blood *109*, 3253-3259.

Kukita, T., Wada, N., Kukita, A., Kakimoto, T., Sandra, F., Toh, K., Nagata, K., Iijima, T., Horiuchi, M., Matsusaki, H.*, et al.* (2004). RANKL-induced DC-STAMP is essential for osteoclastogenesis. J Exp Med *200*, 941-946.

Kuleshov, M. V., Jones, M. R., Rouillard, A. D., Fernandez, N. F., Duan, Q., Wang, Z., Koplev, S., Jenkins, S. L., Jagodnik, K. M., Lachmann, A.*, et al.* (2016). Enrichr: a comprehensive gene set enrichment analysis web server 2016 update. Nucleic Acids Res *44*, W90-97.

Kurotaki, D., Yoshida, H., and Tamura, T. (2020). Epigenetic and transcriptional regulation of osteoclast differentiation. Bone *138*, 115471.

Lamoureux, F., Baud'huin, M., Rodriguez Calleja, L., Jacques, C., Berreur, M., Redini, F., Lecanda, F., Bradner, J. E., Heymann, D., and Ory, B. (2014). Selective inhibition of BET bromodomain epigenetic signalling interferes with the bone-associated tumour vicious cycle. Nat Commun *5*, 3511.

Langfelder, P., and Horvath, S. (2008). WGCNA: an R package for weighted correlation network analysis. BMC Bioinformatics *9*, 559.

Langlais, D., Barreiro, L. B., and Gros, P. (2016). The macrophage IRF8/IRF1 regulome is required for protection against infections and is associated with chronic inflammation. J Exp Med *213*, 585-603.

Le Pape, F., Vargas, G., and Clezardin, P. (2016). The role of osteoclasts in breast cancer bone metastasis. J Bone Oncol *5*, 93-95.

Lee, J. E., Park, Y. K., Park, S., Jang, Y., Waring, N., Dey, A., Ozato, K., Lai, B., Peng, W., and Ge, K. (2017). Brd4 binds to active enhancers to control cell identity gene induction in adipogenesis and myogenesis. Nat Commun *8*, 2217.

LeRoy, G., Rickards, B., and Flint, S. J. (2008). The double bromodomain proteins Brd2 and Brd3 couple histone acetylation to transcription. Mol Cell *30*, 51-60.

Love, M. I., Huber, W., and Anders, S. (2014). Moderated estimation of fold change and dispersion for RNA-seq data with DESeq2. Genome Biol *15*, 550.

Loven, J., Hoke, H. A., Lin, C. Y., Lau, A., Orlando, D. A., Vakoc, C. R., Bradner, J. E., Lee, T. I., and Young, R. A. (2013). Selective inhibition of tumor oncogenes by disruption of super-enhancers. Cell *153*, 320-334.

Miyauchi, Y., Ninomiya, K., Miyamoto, H., Sakamoto, A., Iwasaki, R., Hoshi, H., Miyamoto, K., Hao, W., Yoshida, S., Morioka, H.*, et al.* (2010). The Blimp1-Bcl6 axis is critical to regulate osteoclast differentiation and bone homeostasis. J Exp Med *207*, 751-762.

Nishikawa, K., Nakashima, T., Hayashi, M., Fukunaga, T., Kato, S., Kodama, T., Takahashi, S., Calame, K., and Takayanagi, H. (2010). Blimp1-mediated repression of negative regulators is required for osteoclast differentiation. Proc Natl Acad Sci U S A *107*, 3117-3122.

Park-Min, K. H., Lim, E., Lee, M. J., Park, S. H., Giannopoulou, E., Yarilina, A., van der Meulen, M., Zhao, B., Smithers, N., Witherington, J.*, et al.* (2014). Inhibition of osteoclastogenesis and inflammatory bone resorption by targeting BET proteins and epigenetic regulation. Nat Commun *5*, 5418.

Rahman, S., Sowa, M. E., Ottinger, M., Smith, J. A., Shi, Y., Harper, J. W., and Howley, P. M. (2011). The Brd4 extraterminal domain confers transcription activation independent of pTEFb by recruiting multiple proteins, including NSD3. Mol Cell Biol *31*, 2641-2652.

Ramirez, F., Ryan, D. P., Gruning, B., Bhardwaj, V., Kilpert, F., Richter, A. S., Heyne, S., Dundar, F., and Manke, T. (2016). deepTools2: a next generation web server for deep-sequencing data analysis. Nucleic Acids Res *44*, W160-165.

Raschke, W. C., Baird, S., Ralph, P., and Nakoinz, I. (1978). Functional macrophage cell lines transformed by Abelson leukemia virus. Cell *15*, 261-267.

Roe, J. S., Mercan, F., Rivera, K., Pappin, D. J., and Vakoc, C. R. (2015). BET Bromodomain Inhibition Suppresses the Function of Hematopoietic Transcription Factors in Acute Myeloid Leukemia. Mol Cell *58*, 1028-1039.

Ross-Innes, C. S., Stark, R., Teschendorff, A. E., Holmes, K. A., Ali, H. R., Dunning, M. J., Brown, G. D., Gojis, O., Ellis, I. O., Green, A. R.*, et al.* (2012). Differential oestrogen receptor binding is associated with clinical outcome in breast cancer. Nature *481*, 389-393.

Soysa, N. S., Alles, N., Aoki, K., and Ohya, K. (2012). Osteoclast formation and differentiation: an overview. J Med Dent Sci *59*, 65-74.

Sundaram, K., Nishimura, R., Senn, J., Youssef, R. F., London, S. D., and Reddy, S. V. (2007). RANK ligand signaling modulates the matrix metalloproteinase-9 gene expression during osteoclast differentiation. Exp Cell Res *313*, 168-178.

Takayanagi, H., Kim, S., Koga, T., Nishina, H., Isshiki, M., Yoshida, H., Saiura, A., Isobe, M., Yokochi, T., Inoue, J.*, et al.* (2002). Induction and activation of the transcription factor NFATc1 (NFAT2) integrate RANKL signaling in terminal differentiation of osteoclasts. Dev Cell *3*, 889-901.

Teitelbaum, S. L. (2000). Bone resorption by osteoclasts. Science *289*, 1504-1508.
Troen, B. R. (2006). The regulation of cathepsin K gene expression. Ann N Y Acad Sci *1068*, 165-172.

Wagner, E. F. (2002). Functions of AP1 (Fos/Jun) in bone development. Ann Rheum Dis *61 Suppl 2*, ii40-42.

Whyte, W. A., Orlando, D. A., Hnisz, D., Abraham, B. J., Lin, C. Y., Kagey, M. H., Rahl, P. B., Lee, T. I., and Young, R. A. (2013). Master transcription factors and mediator establish super-enhancers at key cell identity genes. Cell *153*, 307-319.

Wu, H., Xu, G., and Li, Y. P. (2009). Atp6v0d2 is an essential component of the osteoclast-specific proton pump that mediates extracellular acidification in bone resorption. J Bone Miner Res *24*, 871-885.

Yang, M., Birnbaum, M. J., MacKay, C. A., Mason-Savas, A., Thompson, B., and Odgren, P. R. (2008). Osteoclast stimulatory transmembrane protein (OC-STAMP), a novel protein induced by RANKL that promotes osteoclast differentiation. J Cell Physiol *215*, 497-505.

Younesy, H., Nielsen, C. B., Lorincz, M. C., Jones, S. J., Karimi, M. M., and Moller, T. (2016). ChAsE: chromatin analysis and exploration tool. Bioinformatics *32*, 3324-3326.

Yu, C., Niu, X., Jin, F., Liu, Z., Jin, C., and Lai, L. (2016). Structure-based Inhibitor Design for the Intrinsically Disordered Protein c-Myc. Sci Rep *6*, 22298.

Zhang, B., and Horvath, S. (2005). A general framework for weighted gene co-expression network analysis. Stat Appl Genet Mol Biol *4*, Article17.

Zhao, B., Takami, M., Yamada, A., Wang, X., Koga, T., Hu, X., Tamura, T., Ozato, K., Choi, Y., Ivashkiv, L. B.*, et al.* (2009). Interferon regulatory factor-8 regulates bone metabolism by suppressing osteoclastogenesis. Nat Med *15*, 1066-1071.

Zhu, L. J. (2013). Integrative analysis of ChIP-chip and ChIP-seq dataset. Methods Mol Biol *1067*, 105-124.

Zhu, L. J., Gazin, C., Lawson, N. D., Pages, H., Lin, S. M., Lapointe, D. S., and Green, M. R. (2010). ChIPpeakAnno: a Bioconductor package to annotate ChIP-seq and ChIP-chip data. BMC Bioinformatics *11*, 237.

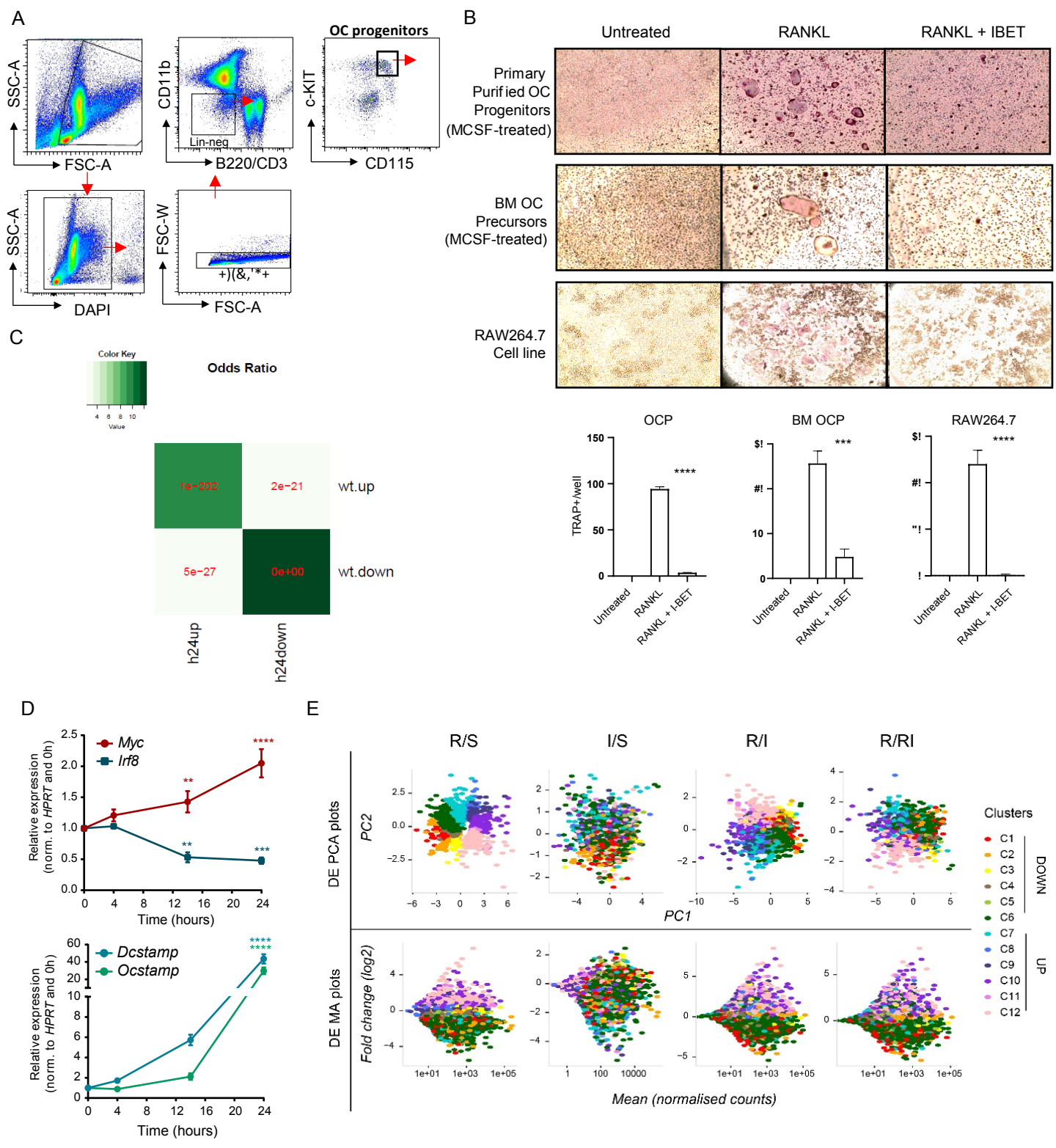

Suppl Figure 1

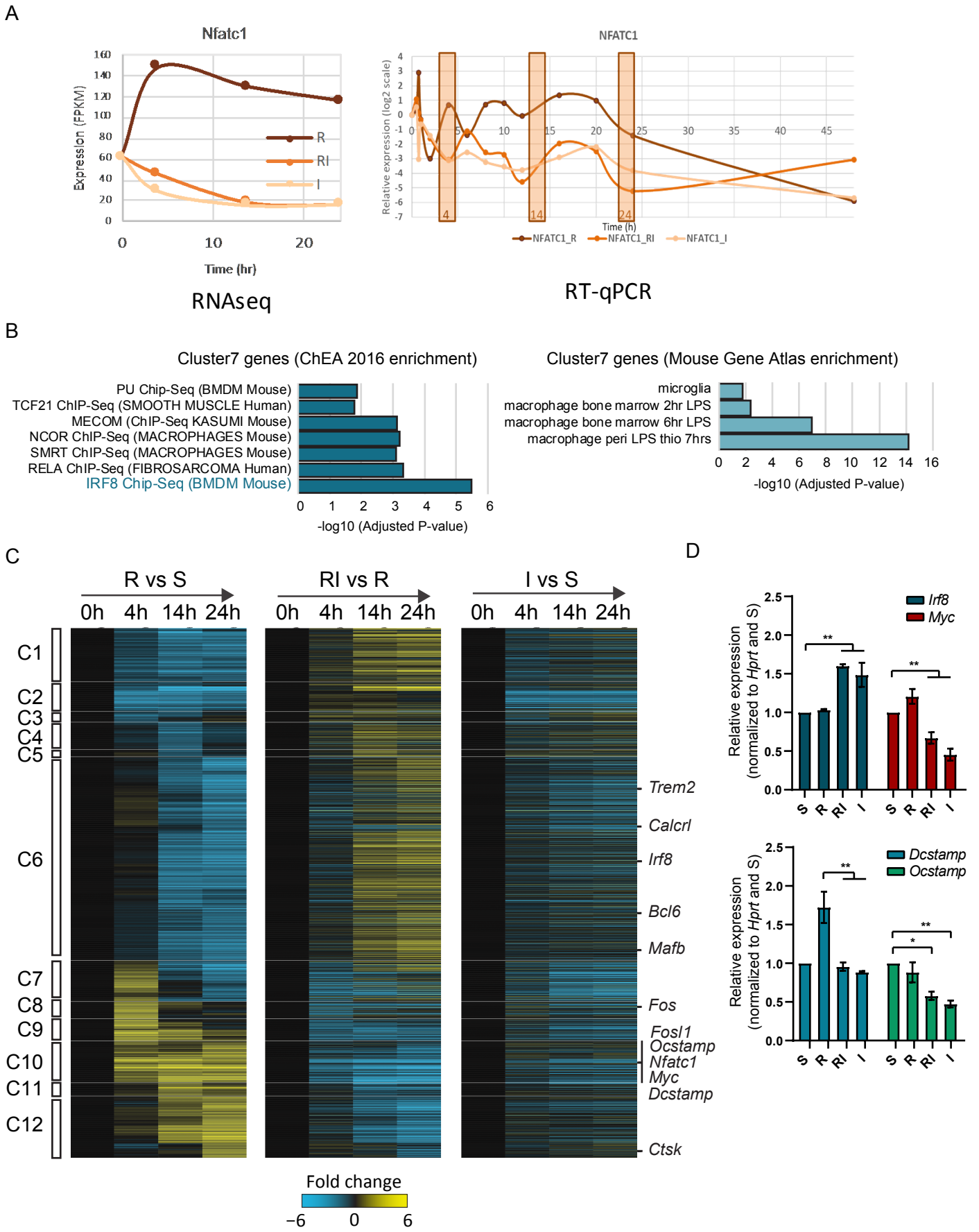

Suppl. Figure 2

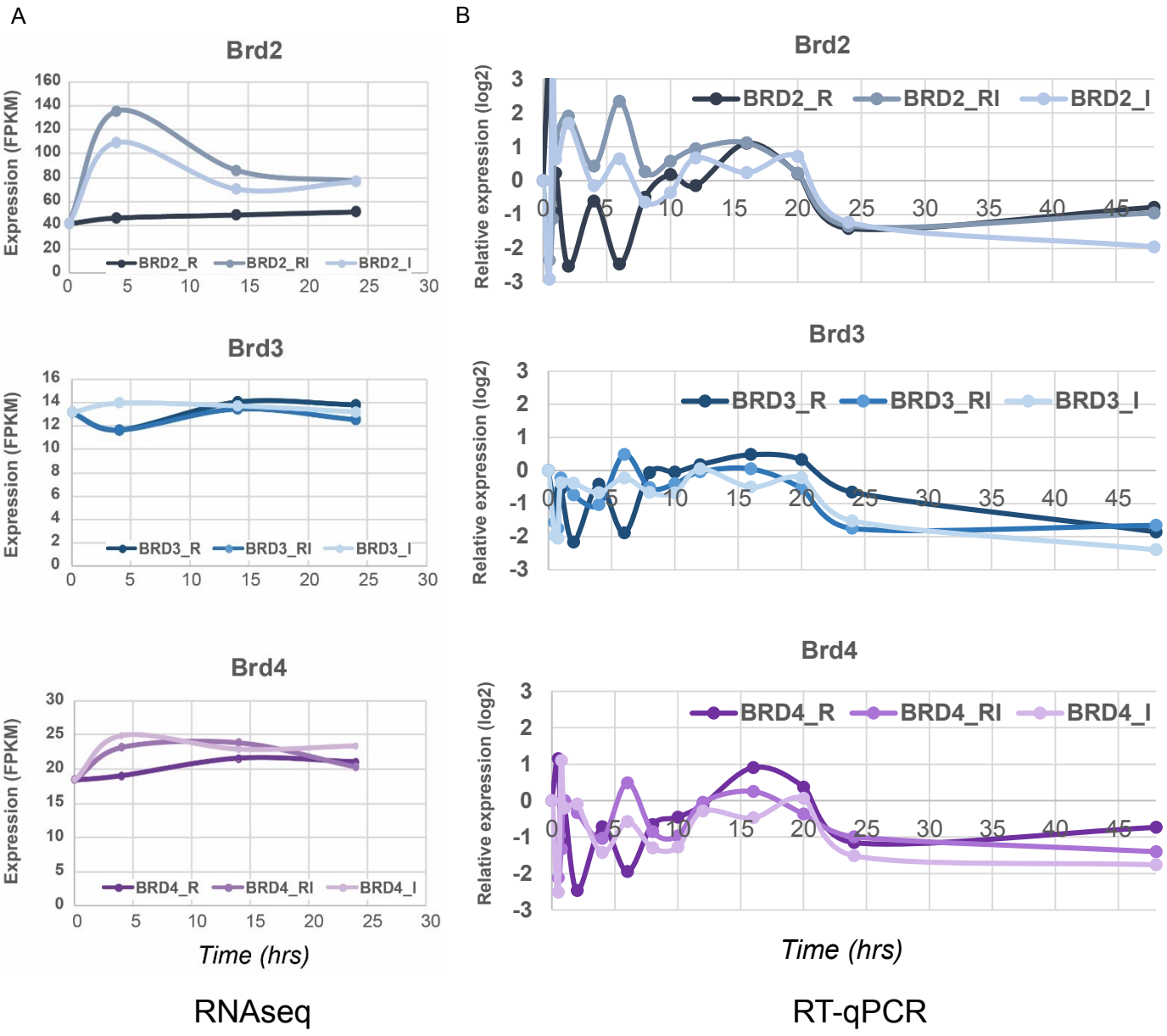

Suppl Figure 3

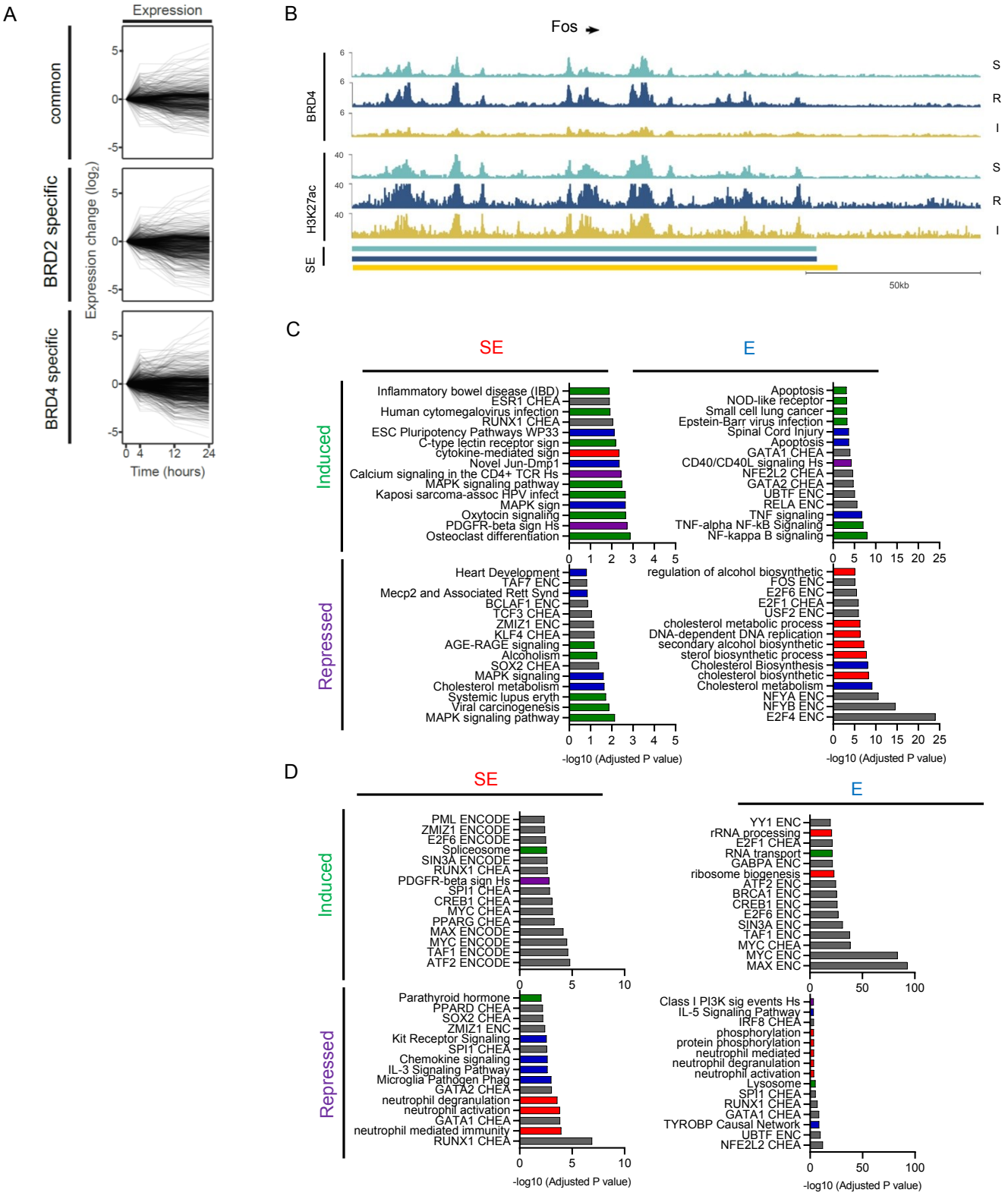

Suppl Figure 4

A

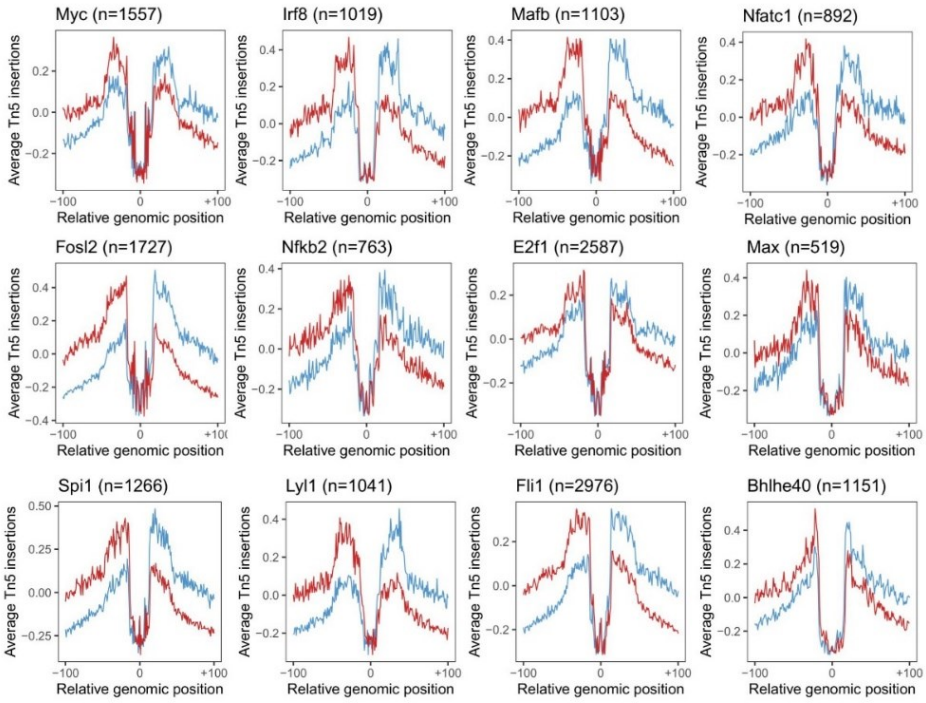

B

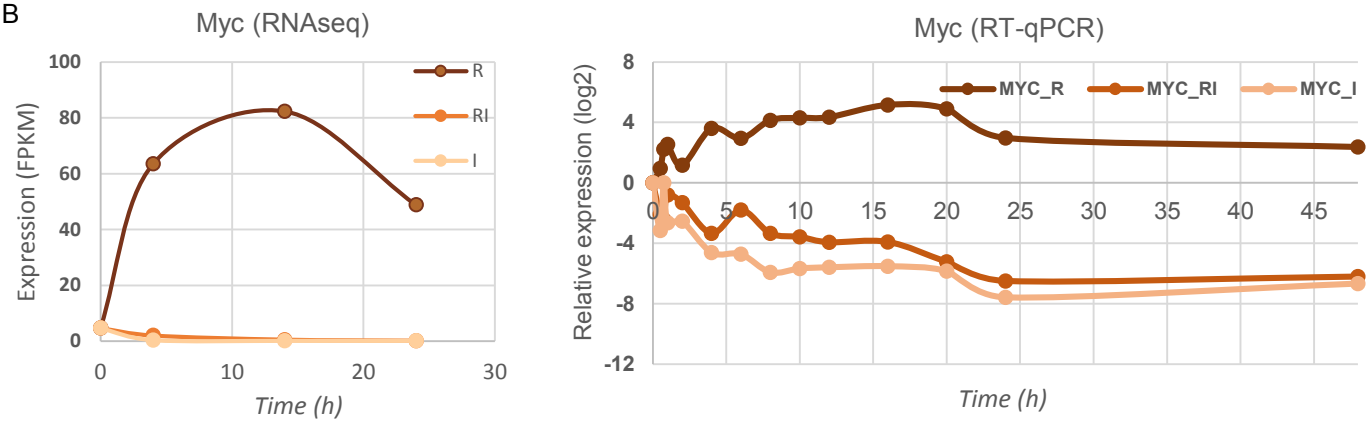

C

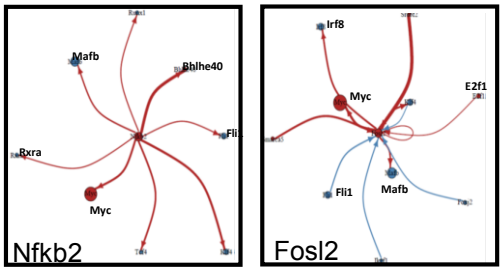

Suppl Figure 5

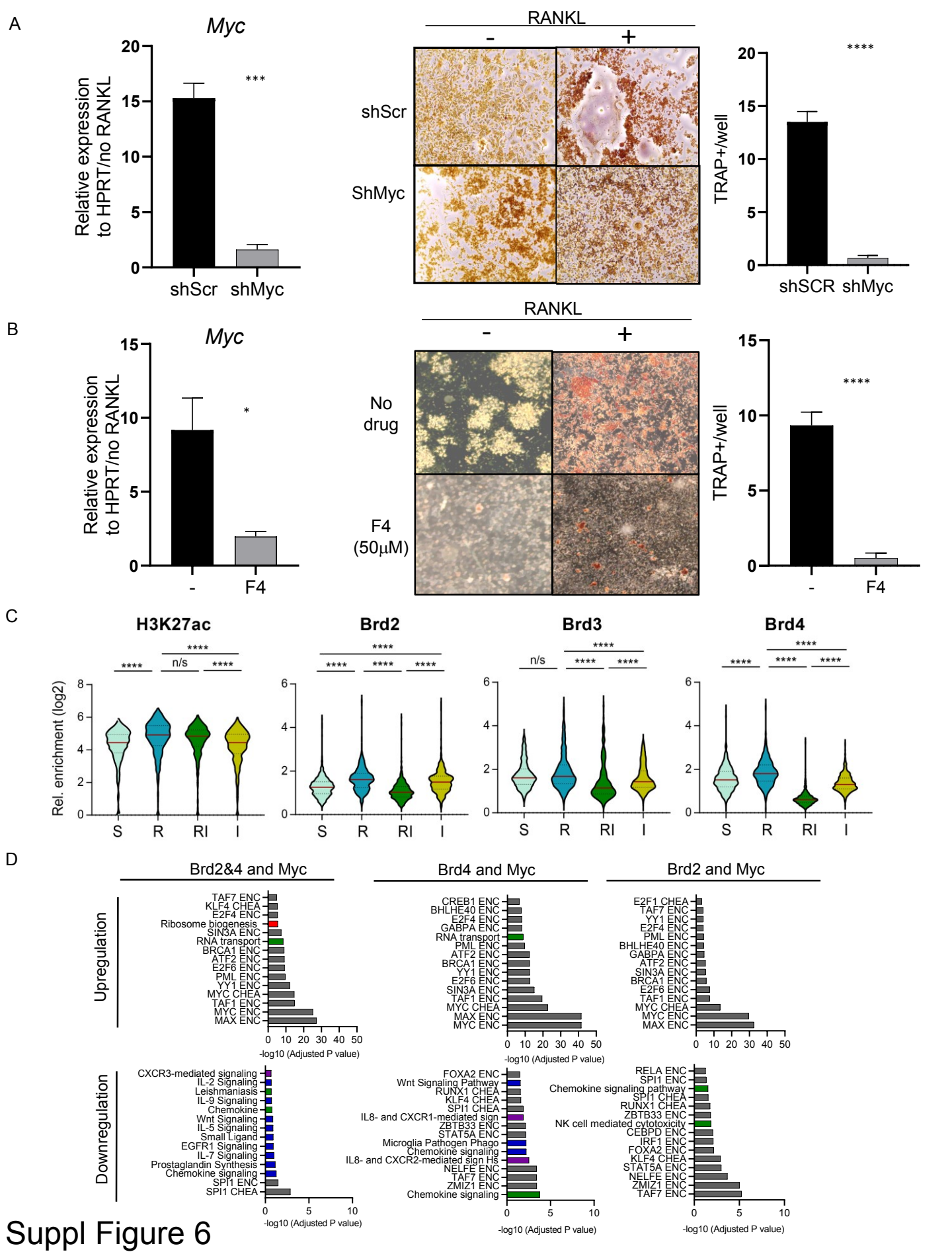

Suppl Figure 6